

## COLD DARK MATTER. II. SPATIAL AND VELOCITY STATISTICS

JAMES M. GELB<sup>1</sup> AND EDMUND BERTSCHINGER

Department of Physics, Massachusetts Institute of Technology, Cambridge, MA 02139

Received 1992 December 25; accepted 1994 May 31

## ABSTRACT

We examine high-resolution gravitational  $N$ -body simulations of the  $\Omega = 1$  cold dark matter (CDM) model in order to determine whether there is any normalization of the initial density fluctuation spectrum that yields acceptable results for galaxy clustering and velocities. Dense dark matter halos in the evolved mass distribution are identified with luminous galaxies; the most massive halos are also considered as sites for galaxy groups, with a range of possibilities explored for the group mass-to-light ratios. We verify the earlier conclusions of White et al. (1987) for the low-amplitude (high-bias) CDM model—the galaxy correlation function is marginally acceptable but that there are too many galaxies. We also show that the peak biasing method does not accurately reproduce the results obtained using dense halos identified in the simulations themselves. The *COBE* anisotropy implies a higher normalization, resulting in problems with excessive pairwise galaxy velocity dispersion unless a strong velocity bias is present. Although we confirm the strong velocity bias of halos reported by Couchman & Carlberg (1992), we show that the galaxy motions are still too large on small scales. We find no amplitude for which the CDM model can reconcile simultaneously the galaxy correlation function, the low pairwise velocity dispersion, and the richness distribution of groups and clusters. With the normalization implied by *COBE*, the CDM spectrum has too much power on small scales if  $\Omega = 1$ .

*Subject headings:* cosmic microwave background — cosmology: theory — dark matter

## 1. INTRODUCTION

The cold dark matter (CDM) model of galaxy formation has had a checkered history. First proposed by Peebles in 1982, the model has the virtue of being relatively well-defined and testable. Assuming  $H_0 = 50 \text{ km s}^{-1} \text{ Mpc}^{-1}$  and  $\Omega = 1$ , the only fundamental free parameter is the overall amplitude of density fluctuations. We characterize this by the conventional quantity  $\sigma_8$ , defined to be the rms density fluctuation, using the linear power spectrum, in a sphere of radius  $800 \text{ km s}^{-1}$ . (See, e.g., Bertschinger 1992 for discussion of this and alternative conventions for the normalization.) Once  $\sigma_8$  is specified the CDM model has, in principle, strong predictive power, although many of the predictions require  $N$ -body and dissipative numerical computations. The complexity of the nonlinear evolution and dissipation has led over the last decade to a lively debate concerning the viability of the CDM model.

In 1985, Davis et al. showed that the CDM model cannot simultaneously fit galaxy clustering (i.e., two-point correlation function) and small-scale velocities (i.e., pairwise velocity dispersion) for any  $\sigma_8$  if dark matter traces galaxies. For  $\sigma_8 = 1$ , motivated by the observation that  $\sigma_8 \approx 1$  for galaxies (Davis & Peebles 1983), the relative velocities of galaxies are predicted to be much larger than observed. The solution proposed by Davis et al. was to decrease the amplitude of density fluctuations by a factor of 2.5 to  $\sigma_8 = 0.4$ , thereby decreasing the pairwise velocity dispersion of galaxies to roughly match observations. In the process, the clustering of galaxies was also diminished. The two-point correlation function was boosted up to the observed range by assuming that galaxies form only in the initially highest density regions, according to the “peak biasing” scheme proposed by Kaiser (1984). Roughly speaking, galaxy density fluctuations were assumed to be 2.5 times the dark matter fluctuations (although peak biasing does not give

an exactly linear relation between galaxies and mass fluctuations). The stronger correlations introduced with biasing compensated for the smaller correlations (and velocities) resulting from lowering the amplitude to  $\sigma_8 = 0.4$ . The paper of Davis et al. (1985, hereafter DEFW) marked the birth of the biased CDM model.

The amplitude of the CDM density fluctuations affects large-scale structure as well as small-scale (20 Mpc and less) clustering and velocities. Many authors have pointed out that the low amplitude of biased CDM is in apparent conflict with large-scale structure. The freedom to vary the biasing (ratio of galaxies to mass) makes it somewhat difficult to pin down these problems. However, large-scale peculiar velocities are particularly useful for testing the normalization because galaxies should trace the same large-scale flows as does dark matter—all bodies accelerate the same way in a gravitational field. Motivated by this fact, Bertschinger & Juszkievicz (1988) tested CDM predictions against the “great attractor” fits of Faber & Burstein (1988) and concluded that CDM with  $\sigma_8 \leq \frac{2}{3}$  was inconsistent with the data. This conclusion was strengthened by analysis of several large-scale galaxy surveys: the angular correlation function of Maddox et al. (1990) from the APM survey; the moments of galaxy counts in cells of Saunders et al. (1991) from the *IRAS/QDOT* survey; and the galaxy density power spectrum from the CfA2 redshift survey by Vogeley et al. (1992).

The large-scale structure measurements indicate a need for more power, hence a larger  $\sigma_8$  if the CDM power spectrum is retained. However, high-amplitude CDM faces the problem of large velocity dispersion noted originally by Davis et al. (1985). A possible solution was suggested by Carlberg & Couchman (1989) and Carlberg, Couchman, & Thomas (1990): velocity bias. They noted that the pairwise velocity dispersion of dark matter halos in high-resolution  $N$ -body simulations is substantially less than that of the mass. This effect was not discovered by Davis et al. because their simulations did not have the

<sup>1</sup> Present address: NASA/Fermilab Astrophysics Center, Fermi National Accelerator Laboratory, P.O. Box 500, Batavia, IL 60510.

resolution needed to find galaxy halos composed of many particles (although it could have been found by White et al. 1987, hereafter WDEF). Couchman & Carlberg (1992) pointed out that with an amplitude corresponding to  $\sigma_8 = 1$ , CDM would do well on large scales, while clustering and velocity biasing might solve the problems on small scales.

However, it is not enough for CDM to predict the correct two-point correlation function and pairwise velocity dispersion of galaxies. It must also predict the correct abundance of galaxies and of galaxy groups as a function of richness. Testing these requires high-resolution numerical simulations. An important first step was taken in 1987 by White et al. They performed a  $P^3M$  simulation, evolved to  $\sigma_8 = 0.4$ , in a 50 Mpc box with enough particles ( $64^3$ ) to study resolved dark matter halos. They found that the evolved halos are, indeed, more strongly correlated than the mass, with the correlation function in reasonable agreement with observations for halos with circular rotation speeds exceeding  $250 \text{ km s}^{-1}$ . However, they found the numbers of halos in their simulations with  $V_{\text{circ}} \geq 100 \text{ km s}^{-1}$ , after breaking up the overly merged massive halos, to be greater than the observed numbers by a factor of 2 or more.

The uncertainty over the correct amplitude for normalizing the CDM (or any other) power spectrum has largely ended with the measurement of the cosmic microwave background anisotropy by Smoot et al. (1992). Their measurements imply  $\sigma_8 \approx 1.1$  (Wright et al. 1992; Efstathiou, Bond, & White 1992; Adams et al. 1993) if the spectrum is scale-invariant as we suppose. Consequently, all standard CDM models with  $\sigma_8 = 0.4$  are obsolete. On the other hand, CDM with  $\sigma_8 = 1$  might be an attractive model if the small-scale velocity bias found by Carlberg et al. is sufficiently strong and if the galaxy numbers and group multiplicities can be made reasonably to match the observations.

In previous work (Bertschinger & Gelb 1991) we have also found a strong velocity bias for halos in the CDM model. However, our interpretation differs somewhat from that of Carlberg (1991); the reduction appears to be a statistical effect, arising because the pairwise velocity statistic weights galaxies by pairs and quadratically by velocities. Therefore, when it is applied to all mass particles, the massive halos in galaxy clusters, with velocities comparable to the cluster dispersion, contribute strongly to the overall pairwise velocity dispersion. When the simulated halos are used, on the other hand, strong merging in the clusters eliminates most of the halos and leaves a single massive object in the center, which has little weight in the pairwise sum. The small number of halos in clusters reduces the pairwise velocity dispersion of halos, but it also leads to clusters with far too few objects to be identified as galaxies.

In a preceding paper (Gelb & Bertschinger 1994, hereafter Paper I), we explored in detail the distribution of simulated halos by circular velocities, and we concluded that no value of  $\sigma_8$  could fully satisfy the constraints given by the number density of galaxies. For any value of  $\sigma_8$  one had too many halos, assuming that circular velocity can be related to luminosity by Tully-Fisher and Faber-Jackson relations. However, these results are limited by the fact that the  $N$ -body simulations we used lack gas, so it is worthwhile making other tests of the model, with generous allowance for uncertainties in how galaxies are related to dark matter halos.

Dissipationless simulations like ours have the disadvantage of being unable to correctly model the process of galaxy forma-

tion inside dark matter halos. By necessity, we assume that galaxies form only inside dark matter halos. This assumption appears to be confirmed by gas dynamical simulations (e.g., Katz, Hernquist, & Weinberg 1992; Cen & Ostriker 1992a, b; Evrard, Summers, & Davis 1994), which also support our conclusions concerning the degree of velocity biasing. Why then should we continue with dissipationless simulations? The reason is dynamic range. With simulations including gravity only, we are able to resolve galaxy halos in volumes up to 100 Mpc on a side, large enough to capture the long-wavelength density fluctuations important for high-amplitude CDM (cf. Paper I). Gas dynamical simulations with equal numbers of particles are still prohibitively expensive. The volumes studied to date with high-resolution gas dynamical simulations have been too small to include all important dynamical effects.

In this paper we study spatial clustering and velocity statistics of dark matter halos in the CDM models using high-resolution  $N$ -body simulations. The principle goal is to answer the question: is there a normalization  $\sigma_8$  such that the two-point spatial correlation function of the resolved halos and the pairwise velocity dispersion of the resolved halos matches the observations? This question is addressed by analyzing the particle-mesh and particle-particle/particle-mesh ( $P^3M$ )  $N$ -body simulations discussed in Paper I. For economy of notation (see Paper I) we refer to the simulations as CDM  $n(N^3, L, R_{1/2})$ . The numbers in parentheses indicate the following simulation parameters: (1)  $N^3$  particles, (2) a comoving box of length  $L$  Mpc on a side, and (3) a comoving force softening length of  $R_{1/2}$  kpc. The force softening is characterized by  $r = R_{1/2}$ : where  $r^2 F_r / (Gm^2) = \frac{1}{2}$ , i.e., half its Newtonian value.

Our studies focus on the simulation CDM 16( $144^3, 100, 85$ ). The comoving Plummer softening length is  $\epsilon = 65$  kpc and the particle mass is  $m_{\text{part}} = 2.3 \times 10^{10} M_{\odot}$ . Of all our simulations (see Gelb 1992, Appendix II), this simulation has the best compromise of mass and force resolution in a 100 Mpc box. A relatively large box is required to adequately represent waves in the initial conditions, particularly for evolution up to  $\sigma_8 = 1$  (see Paper I and §§ 2.1 and 2.2 below). We will examine positions and peculiar velocities at several amplitudes:  $\sigma_8 = 0.4, 0.5, 0.7$ , and 1.0. Each epoch studied is considered a candidate for the present day; i.e., we test whether spatial and velocity statistics match the observations. The box length is assumed to have a physical length of 100 Mpc for CDM 16 with a Hubble constant  $H_0 = 50 \text{ km s}^{-1} \text{ Mpc}^{-1}$  (and  $\Omega = 1$ ) at each candidate epoch.

We will begin by exploring some background material: box size, the standard CDM model, massive halos, and velocities in § 2. We then briefly discuss some limitations of the method of peak particles and argue the necessity of using resolved halos to study the CDM model in § 3. In § 4 we study the two-point correlation function of simulated galaxies, while in § 5 we study the abundance and richness distribution of galaxy groups. In both cases the results depend on how overmerged halos are broken apart, a point that we investigate in some detail. In § 6 we investigate the small-scale velocity statistics of the galaxies. In § 7 we summarize the implications for the  $\Omega = 1$  CDM model. Further numerical details can be found in Bertschinger & Gelb (1991), Gelb (1992), and Paper I.

## 2. BACKGROUND AND THE STANDARD MODEL

In this section we explore the issue of box size; we test whether we can reproduce the results of WDEF; and we consider complications arising from massive halos and from defi-

nitions of halo velocities. We will confirm that the “standard” biased CDM model ( $\Omega = 1$ ,  $\sigma_8 = 0.4$ ) produces far too many halos compared with the observations.

### 2.1. Box Size: Mass Correlation Length

We are interested in studying models evolved to  $\sigma_8 = 1$ . More highly evolved models require larger boxes since successively larger waves begin to go nonlinear. In this subsection we examine linear theory predictions regarding the importance of long waves in the initial conditions. We then present nonlinear results using evolved  $N$ -body simulations to study the dependence on box size of the two-point correlation function and the pairwise velocity dispersion of the mass.

In Figure 1a we show the linear, rms mass fluctuation in a sphere of radius  $8h^{-1} = 16$  Mpc. We normalize the Holtzman (1989) (5% baryons) CDM power spectrum so that  $\sigma_8 = 1$ . We then compute  $\sigma_8(\lambda_{\max})$  by including only waves with wavelength less than  $\lambda_{\max}$  in the numerical integration of  $\sigma_8$ . The value of the maximum wavelength represented in a simulation computed in a box of length  $L$  on a side is  $\lambda_{\max} = L$ . As  $\lambda_{\max} \rightarrow \infty$ ,  $\sigma_8(\lambda_{\max}) \rightarrow 1$  by definition. We show vertical bars at  $\lambda_{\max} = 51.2$  Mpc and 100 Mpc, the sizes of several of our simulation cubes.

For  $\lambda_{\max} = 51.2$  Mpc we find  $\sigma_8(\lambda_{\max}) \approx 0.6$ . For  $\lambda_{\max} = 100$  Mpc we find  $\sigma_8(\lambda_{\max}) \approx 0.9$ . For  $\lambda_{\max} = 150$  Mpc we find  $\sigma_8(\lambda_{\max}) \approx 0.98$  and it quickly approaches unity thereafter. We conclude that long waves (with  $\lambda > 50$  Mpc) make significant contributions to  $\sigma_8$  and, by extension, to the correlation length  $r_0$  (where the two-point correlation function  $\xi = 1$ ). Therefore, we expect that the nonlinear evolution of our  $N$ -body simulations up to the amplitude  $\sigma_8 = 1$  will result in a serious underestimate of  $r_0$  in 51.2 Mpc boxes but probably not in 100 Mpc boxes.

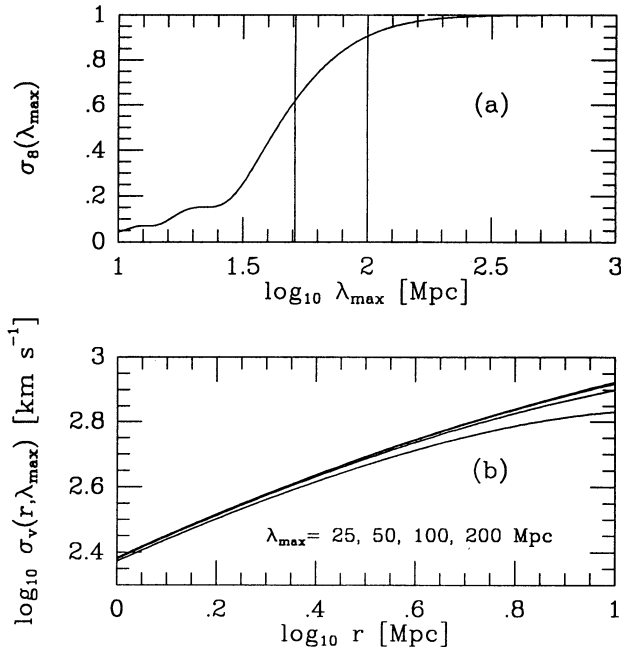


FIG. 1.—(a) Linear theory predictions for  $\sigma_8$  as a function of box size  $\lambda_{\max}$ . The power spectrum (Holtzman 1989, 5% baryons) is normalized so that  $\sigma_8 = 1$  when  $\lambda_{\max} \rightarrow \infty$ . (b) Linear theory predictions for three-dimensional pairwise velocity dispersions,  $\sigma_v$ , as a function of box size,  $\lambda_{\max}$ , and separation  $r$ , for four values of  $\lambda_{\max}$ .

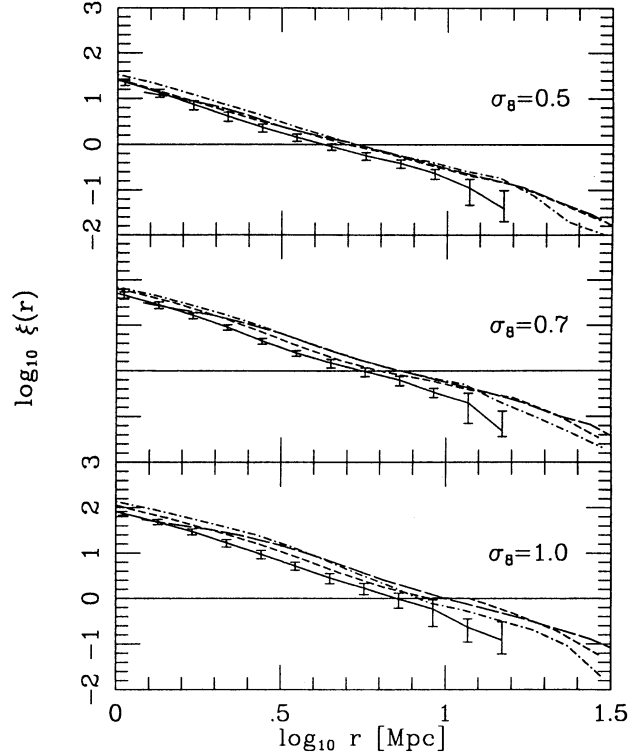


FIG. 2.— $\log_{10} \xi(r)$  (mass) vs.  $\log_{10} r$  where  $r$  is measured in comoving Mpc for various simulations in boxes ranging from 51.2 Mpc on a side to 400 Mpc on a side. The five  $128^3$  particle PM simulations ( $R_{1/2} = 280$  kpc, 51.2 Mpc box) are averaged together (solid curves) with  $1 \sigma$  error bars. The other simulations are CDM 11( $128^3$ , 102.4, 560; dot-dashed curves), CDM 16( $144^3$ , 100, 85; short-dashed curves), and CDM 10( $128^3$ , 400, 2188; long-dashed curves). Note that  $\xi(r)$  is underestimated in the 51.2 Mpc boxes.

To test the above prediction, in Figure 2 we show  $\xi(r)$  for various simulations for the mass (particles). The important parameter for our discussion is the box size. The plots show that the correlation length  $r_0$  grows roughly linearly with  $\sigma_8$  from 5 Mpc at  $\sigma_8 = 0.5$  to 10 Mpc at  $\sigma_8 = 1$  for the simulations in larger boxes. We must match the observations with the simulated halos, not the mass, unless the halos trace the mass. However, we expect the same waves that affect the mass will also affect halo clustering. We notice in Figure 2 that the 51.2 Mpc box simulations underestimate the correlation length (by about 30% for  $\sigma_8 = 1$ ) when compared with the simulations in  $\geq 100$  Mpc boxes. The underestimate is greater for increasing  $\sigma_8$  (being about 20% for  $\sigma_8 = 0.5$ ), as expected. Boxes smaller than 50 Mpc on a side are too small to get the correlation length correct to better than 10% even for an amplitude as small as  $\sigma_8 = 0.4$ . However, we find that a 100 Mpc box is sufficiently large, as the correlation length (10 Mpc) agrees with the results from the 400 Mpc box simulation, despite the poor resolution (2 Mpc) of the latter.

From Figure 2 we can also examine the simulation-to-simulation variation in the value of  $r_0$ . We see basic agreement in  $r_0$  among the larger box simulations. However, we do see a smaller value in  $r_0$  at  $\sigma_8 = 0.7$  for CDM 16 (100 Mpc box) indicating that there are simulation-to-simulation fluctuations. The fluctuations for the five  $R_{1/2} = 280$  kpc PM simulations in 51.2 Mpc boxes are shown with  $1 \sigma$  error bars. The largest fluctuations are found on the largest scales.



We conclude that the 51.2 Mpc boxes are too small for accurate predictions of the two-point correlation functions particularly for larger values of  $\sigma_8$ . It is unfortunate that CDM 16 (100 Mpc box) has a slight sag on scales near 10 Mpc owing to statistical fluctuation. This will limit some of the conclusions we can draw from this single simulation. Nevertheless, the large numbers of halos in this large box provide a fair test of the CDM model. More realizations would be helpful, but our other  $\sim 100$  Mpc box simulations have poor force and mass resolution.

### 2.2. Box Size: Mass Pairwise Velocity Dispersion

In this subsection we examine the effect of the box size on the pairwise velocity dispersion  $\sigma_p(r)$  as a function of galaxy separation:

$$\sigma_p^2(r) \equiv \frac{1}{3} \langle (v_2 - v_1)^2 \rangle, \quad (2.1)$$

where the average is taken over pairs of particles (for the mass) or halos separated by distance  $r = |\mathbf{r}_1 - \mathbf{r}_2|$ , with peculiar velocities  $\mathbf{v}_1$  and  $\mathbf{v}_2$ . Nonlinear studies of velocity dispersions are the subject of Gelb, Gradwohl, & Frieman (1993).

For an initial estimate of effects of finite box size we consider the linear theory prediction for the three-dimensional pairwise dispersion  $\sigma_v(r) = 3^{1/2} \sigma_p(r)$ . We evaluate this quantity using the  $\sigma_8 = 1$  linear normalization, with a wavelength cutoff  $\lambda_{\max}$  applied to the numerical integration (as we did in § 2.1) to mimic the effect of a finite box size. The results are shown in Figure 1b. We see there is a significant difference between a 25 Mpc box and a 50 Mpc box (particularly for larger values of  $r$ ) and a smaller difference between a 50 Mpc box and a 100 Mpc box. The results converge on the scales of interest in this paper, i.e.,  $r \sim 1\text{--}10$  Mpc, for  $\lambda_{\max} \gtrsim 100$  Mpc.

In Figure 3 we show  $\sigma_p(r)$  for the mass for the same simulations studied in § 2.1. We notice that the velocities are higher for the simulations in boxes of size  $\geq 100$  Mpc than for the simulations in 51.2 Mpc boxes—long waves in the initial conditions affect nonlinear pairwise velocities on smaller scales (see also Gelb et al. 1993). We see that 100 Mpc boxes are sufficient because the results for the 400 Mpc box simulation are comparable to the other 100 Mpc box simulations. The 400 Mpc box simulation has extremely soft forces ( $R_{1/2} = 2$  Mpc) so the velocities are actually lower than in the 100 Mpc simulations. (The parameters in the 400 Mpc simulation are close to the values used by Park 1990.) We use our results from linear theory to strengthen our argument that a 100 Mpc box is sufficient for studying the velocities. This is encouraging because we demonstrated in the previous section that a 100 Mpc box is sufficient for studying spatial correlations.

### 2.3. The Standard Biased CDM Model: $\sigma_8 = 0.4$

In the above sections we found that a box of size 51.2 Mpc is too small to include all the long-wavelength contributions important for clustering and pairwise velocity dispersions on small scales. However, much of the past work has been done using simulations of this size or smaller. To show that our simulations are consistent with previous work, we perform two simulations with parameters similar to those used by WDEF. These P<sup>3</sup>M simulations, CDM 12 and CDM 13, use  $64^3$  particles in 51.2 Mpc boxes with Plummer softening  $\epsilon = 40$  kpc comoving. The particle mass is  $m_{\text{part}} = 3.5 \times 10^{10} M_\odot$ . For comparison, WDEF computed three  $64^3$  particle P<sup>3</sup>M simulations in 50 Mpc boxes with force resolution  $\sim 50$  kpc comoving (they used a linear sphere density profile). We study the

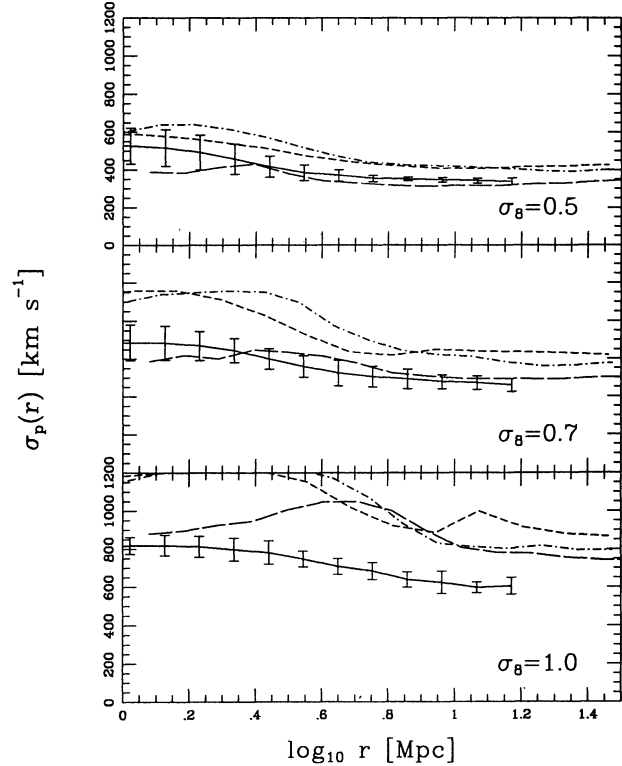


FIG. 3.— $\sigma_p(r)$  for the mass for the cases considered in Fig. 2

models at  $\sigma_8 = 0.4$ , the normalization advocated by DEFW. To identify dark matter halos we use two different prescriptions: DENMAX (our density maxima finder, see Paper I) and FOF (friends-of-friends); WDEF used the latter. For FOF we report the linking length,  $l$ , in units of the mean interparticle spacing. We study the numbers of simulated halos and we break up the massive halos into clusters to study the effect on the spatial clustering of massive halos with circular velocities  $V_{\text{circ}} \geq 250 \text{ km s}^{-1}$ .

In Table 1 we list the numbers of halos with  $V_{\text{circ}} \geq 100, 200,$  and  $250 \text{ km s}^{-1}$ . The results are shown for averages from CDM 12( $64^3, 51.2, 52$ ) and CDM 13( $64^3, 51.2, 52$ ) (two different sets of initial random numbers) and for averages from WDEF. (We divide their numbers by three since they report totals for three simulations. We also scale their numbers in a 50 Mpc box to a 51.2 Mpc box.) In computing observational estimates we characterize all our halos by their circular velocities, and we relate observed estimates of one-dimensional velocity dispersions,  $\sigma_1$ , to circular velocities by

$$\sigma_1 = F \frac{V_{\text{circ}}}{\sqrt{3}}. \quad (2.2)$$

We report our observational estimates for  $F = 1$  and  $F = 1.1$  (see Paper I) and those of WDEF for  $F = 1$  (in our notation). WDEF used  $F = 1$  but in a subsequent paper at  $\sigma_8 = 0.4$  they used  $F = 1.1$  (see Frenk et al. 1988). We demonstrated in Paper I that  $F = 1.1$  works better for  $\sigma_8 = 0.5$  compared with larger values of  $\sigma_8$ . In any event,  $F = 1.1$  lowers the observational estimates, making the disparity with the observations worse. The observational estimates of WDEF are higher than ours. This stems from the fact that they used a different Faber-Jackson relationship for ellipticals. We note

TABLE 1  
NUMBERS OF HALOS IN 51.2 Mpc BOX P<sup>3</sup>M SIMULATIONS AT  $\sigma_8 = 0.4$

Data Set	FOF( $l = 0.1$ )	FOF( $l = 0.2$ )	DENMAX	Breakup
$\langle$ CDM 12/13 $\rangle^a$	848, 169, 80	954, 127, 53	1092, 177, 89	1292, 353, 241
Observational estimate, $F = 1.0$ (616, 168, 83) <sup>b</sup>				
Observational estimate, $F = 1.1$ (592, 151, 70) <sup>b</sup>				
WDEF <sup>c</sup>				Before breakup 1362, 202, — After breakup 2844, 365, —
Observational estimate, $F = 1.0$ (945, 220, —)				

<sup>a</sup> Average of the two simulations.

<sup>b</sup> Observational estimate assuming  $F$  for eq. (2.2). Triplets of integers are for  $V_{\text{circ}} \geq 100$  km s<sup>-1</sup>, 200 km s<sup>-1</sup>, and 250 km s<sup>-1</sup>.

<sup>c</sup> Average of three 50 Mpc simulations from White et al. (1987) scaled to a 51.2 Mpc box.

that the Faber et al. (1989) survey of ellipticals has even fewer bright ellipticals (factor  $\sim \frac{1}{2}$  for  $\sigma_1 \geq 350$  km s<sup>-1</sup>) than we get with our Faber-Jackson relation,  $M_{B_T} = -6.6364 \log_{10}(\sigma_1) - 5.884$ . The differences are not critical since we will find, using either our estimates or those of WDEF, that there are too many simulated halos compared with the observations. WDEF studied the clustering of halos with  $V_{\text{circ}} \geq 250$  km s<sup>-1</sup> but they report only numbers for  $V_{\text{circ}} \geq 100$  and 200 km s<sup>-1</sup>, so the entry for 250 km s<sup>-1</sup> is unfilled in Table 1.

The triplet of numbers in Table 1 are for  $V_{\text{circ}} \geq 100, 200, 250$  km s<sup>-1</sup>. Results are shown for halos defined using FOF and DENMAX, and for DENMAX after breaking up the massive halos into groups and clusters of halos (see §§ 4.2 and 4.3). The WDEF results are shown before and after their special treatment of merging. Observational estimates are given in the first column.

We identify halos in our simulations with FOF linking lengths  $l = 0.1$  and 0.2, and DENMAX with a 512<sup>3</sup> density grid. Circular velocities are defined at a comoving radius of 150 kpc. We find similar results using different DENMAX grids and different radius cuts (see Paper I). The variation in the numbers from CDM 12 versus CDM 13 are less than 10%. We see from Table 1 that the results for the DENMAX analyses are closer to the FOF ( $l = 0.1$ ) case than the FOF ( $l = 0.2$ ) case for the larger circular velocity cutoffs. WDEF reported their results before and after their prescription for restoring merged halos into clusters. They used FOF with an unspecified, small linking parameter and they defined their circular velocities using a mass within a sphere of mean density 1000 times the present critical density. Despite these differences, we find reasonable agreement for the numbers of halos with  $V_{\text{circ}}$  exceeding 200 km s<sup>-1</sup>. However, their break-up procedure results in more than twice as many halos as we find for  $V_{\text{circ}} \geq 100$  km s<sup>-1</sup>. In any case, the simulations predict more than twice as many halos as there ought to be.

In Figure 4 we show averages of the two-point correlation functions from the two P<sup>3</sup>M simulations for the halos with  $V_{\text{circ}} \geq 100, 200,$  and 250 km s<sup>-1</sup> at  $\sigma_8 = 0.4$ . The mass is shown as a solid curve (also with 1  $\sigma$  error bars in the bottom panel). Our mass correlation length agrees with WDEF:  $r_0 \approx 4$  Mpc. We show the observed two-point correlation function ( $r_0 = 10$  Mpc; logarithmic slope  $-1.8$ ) as a straight solid line. We see a slight enhancement of the correlation length of the halos (dotted and dashed curves) compared with the correlation length of the mass. WDEF reported a similar enhancement. The two-point correlation function also has the wrong shape; in agreement with WDEF it is too steep on small scales and has a sag at  $r \sim 1.5$  Mpc.

The enhancement in  $\xi$  for the bright halos is not large enough to reconcile  $\sigma_8 = 0.4$  with the observations. WDEF argued, and we present more arguments later, that the massive halos might represent clusters of galaxies that have merged. WDEF, in a complicated manner, found every halo that ever formed in the evolution of their models and then used a prescription for merging. (Rather than mimic their procedure in detail, we simply add halos to each massive system in proportion to its bound mass.) When WDEF applied their algorithm to their models, they found significantly more sites for galaxy formation compared with not breaking up the massive halos. (We list their numbers as *before* and *after* in the “breakup”

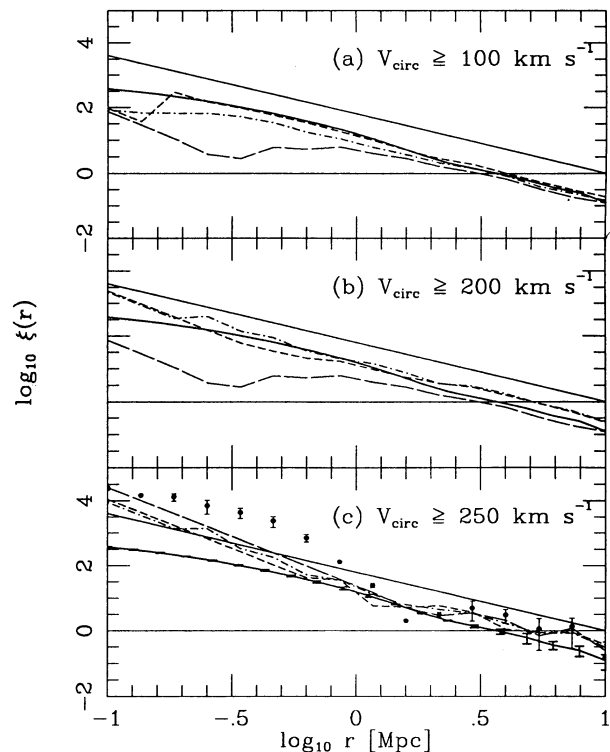


FIG. 4.—Average  $\log_{10} \xi(r)$  for resolved halos with (a)  $V_{\text{circ}} \geq 100$  km s<sup>-1</sup>, (b)  $V_{\text{circ}} \geq 200$  km s<sup>-1</sup>, and (c)  $V_{\text{circ}} \geq 250$  km s<sup>-1</sup> from two 64<sup>3</sup> particle, P<sup>3</sup>M simulations with  $\epsilon = 40$  kpc and 51.2 Mpc boxes. The solid curves are for the mass (1  $\sigma$  error bars are shown in the bottom panel) and the solid lines are the observed  $\xi$ . The results are shown for halos found with FOF ( $l = 0.1$ ; short-dashed curves) and FOF ( $l = 0.2$ ; long-dashed curves) and DENMAX (512<sup>3</sup> grid; dot-dashed curves). In the bottom panel we also show points (with 1  $\sigma$  error bars) for catalogs with the massive halos broken up.

column of Table 1.) They found  $\xi$  is significantly enhanced after breakup, and halos with  $V_{\text{circ}} \geq 250 \text{ km s}^{-1}$  then matched the observed  $\xi$  fairly well. If one adds halos to massive systems one gives extra weight to these systems which are more correlated than smaller systems, thereby increasing the correlation function (Kaiser 1984).

We show our results with the breakup of massive halos as points in the bottom panel of Figure 4. We show  $1 \sigma$  error bars from the two simulations. This procedure introduces new small-scale pairs enhancing  $\xi$  on small scales. We find for one of our simulations that  $\xi$  comes close to the observed line and that for the other simulation the enhancement at large  $r$  is small. We find that  $r_0$  for the mass has a substantial simulation-to-simulation fluctuation at  $r \sim 10 \text{ Mpc}$  which is not surprising in a small box (see Fig. 2). The larger correlation length of the halos corresponds to the simulation with the larger correlation length in the mass. Giving extra weight to the massive halos enhances  $\xi$  provided that there are significant contributions to  $\xi$  from long wavelengths.

Our crude break-up scheme is less ambitious than that of WDEF and it produces fewer halos. We include it here only to illustrate the points made by WDEF and to emphasize the problem associated with producing too many halos. In agreement with WDEF, we find that it is essential to break up the massive halos in order to approximately reconcile the two-point correlation function of resolved halos at  $\sigma_8 = 0.4$  with the observed two-point correlation function. However, if we break up the massive halos enough to enhance  $r_0$  to match the observations, then the resulting numbers of halos far exceed the observational estimates. Moreover  $\xi(r)$  still has the wrong shape. These facts must be considered to be serious shortcomings of the model. The discrepancies must be considered tentative, however, because we know that a 51.2 Mpc box is too small. We use a 100 Mpc box in subsequent sections.

#### 2.4. Halo Velocities

In this subsection we present a few comments concerning the velocities of resolved halos. This subject is important for assessing velocity bias: the pairwise velocity dispersion of the halos can much be less than that of the mass (see Carlberg, et al. 1990). In Figure 5 we show  $\sigma_p(r)$  at  $\sigma_8 = 0.7$  for CDM 12(64<sup>3</sup>, 51.2, 52) for the mass and for the halos (found with a 512<sup>3</sup> DENMAX grid). We use the center of momentum to define the velocities of the halos. We see that  $\sigma_p$  is significantly smaller for the halos than for the mass. One possible source of this “velocity bias” is dynamical friction of the halos with the surrounding medium (Carlberg et al. 1990), where the internal motions of particles in the halo exchange energy and momentum with surrounding particles or other halos.

Much of the velocity bias, however, might actually be a statistical effect. To see this, in Figure 5 we also show  $\sigma_p$  for the mass with the particles from the two largest halos removed (*dashed-dotted curve*). These large halos have circular velocities (defined with  $R = 150 \text{ kpc}$  comoving) of  $981 \text{ km s}^{-1}$  and  $904 \text{ km s}^{-1}$ . We remove all of the DENMAX particles—even the unbound ones—which involve 7719 particles and 4603 particles, respectively. Removal of these particles is unrelated to dynamical friction. We see that the mass pairwise velocity dispersion is reduced significantly by this removal, and therefore the amount of dynamical friction required to explain the overall velocity bias is less than one might expect. The reason why removing the massive halos has such a large effect on  $\sigma_p$  is simple (Bertschinger & Gelb 1991). The calculation of  $\sigma_p$  for

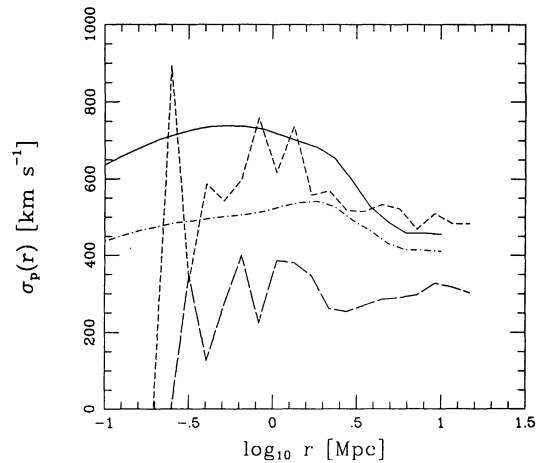


FIG. 5.— $\sigma_p(r)$  at  $\sigma_8 = 0.7$  from CDM 12(64<sup>3</sup>, 51.2, 52). The solid curve is for the mass. The dot-dashed curve is for the mass with the particles from the two largest halos removed. The result for the DENMAX halos with  $V_{\text{circ}} \geq 192 \text{ km s}^{-1}$  is the long-dashed curve. The result using the velocity of the maximally bound particle in a halo rather than the center of momentum of the halo is the short-dashed curve.

the particles weights each pair, giving quadratically greater weight to pairs of the most massive halos. The pairwise velocity dispersions of these large objects are also much higher than they are for smaller systems. If we remove large halos we remove a large number of pairs of high-velocity particles.

We now consider the important distinction between using the velocity of the maximally bound particle from a halo (used by WDEF) and the center-of-momentum velocity. The short dashed curve in Figure 5 is  $\sigma_p$  for the halos with  $V_{\text{circ}} \geq 192 \text{ km s}^{-1}$ , but we use the velocity of the maximally bound particle; i.e., the one with the minimum potential computed by direct summation of particles in the halo treated in isolation. By using the center of momentum for the velocity of the halo rather than the velocity of the maximally bound particle, we get lower values of  $\sigma_p$  because individual particles have a significant velocity dispersion about the mean halo velocity; i.e., we are not including the internal halo velocity dispersion when we use the center of momentum. It makes sense to define the velocity of a halo using the center of momentum of the halo because observers define redshifts using the average velocities of the stars in a galaxy.

### 3. PEAK PARTICLES

In this section we discuss an alternative definition of “galaxies” based on particles initially in density peaks. This method is often used with  $N$ -body simulations lacking sufficient mass or force resolution to resolve evolved dark matter halos (see Kaiser 1984; DEFW; Bardeen et al. 1986; Park 1990, 1991; Katz, Quinn, & Gelb 1993). Galaxies are identified as particles nearest initial (linear) density maxima and their evolution is followed along with the other particles representing intergalactic clouds of dark matter. Only peaks with density exceeding some threshold are accepted. The peak threshold, for a given Gaussian smoothing radius used to smooth the initial density field, is chosen to give the correct number of bright halos in the simulation volume.

#### 3.1. The Two-Point Correlation Function: $\xi(r)$

Following Frenk et al. (1988), we use Gaussian smoothing radii  $R_s$  of 550 kpc comoving and 880 kpc comoving, with



corresponding density fluctuation thresholds  $\nu = 2.6$  and  $3.0$  (for  $R_s = 550$  kpc comoving and  $\nu = 2.0$  and  $2.5$  (for  $R_s = 880$  kpc comoving) in units of  $\sigma_p$ —the density dispersion computed from the smoothed, initial density field. These values of  $\nu$  give roughly 700 and 1600 galaxies, respectively, in a  $(100 \text{ Mpc})^3$  volume (our simulation CDM 16). Using the parameters in the Schechter luminosity function (see Paper I where we used parameters from Efstathiou, Ellis, & Peterson 1988), these correspond to circular velocity cutoffs of approximately  $250 \text{ km s}^{-1}$  and  $200 \text{ km s}^{-1}$ , respectively. For a given Gaussian smoothing radius smaller values of  $\nu$  correspond to smaller circular velocity cutoffs. We choose two values of  $R_s$  to test the sensitivity of our results to this parameter.

We next determine  $\xi$  computed using only the peak particles in the CDM 16 simulation. In other words, we compute the two-point correlation function using the present positions of the particles which are tagged as galaxies. The results are shown in Figure 6. The peak particles indicate that  $\sigma_8 = 0.5$  is possibly suitable as the present epoch—the value of  $r_0$  is roughly 10 Mpc and the logarithmic slope is very nearly  $-1.8$  from about 1 Mpc to 20 Mpc. Note that this success is exactly what led DEFW to champion biased CDM. The correlation lengths for  $\sigma_8 = 0.7$  and  $\sigma_8 = 1.0$  are also roughly 10 Mpc, but the slope steepens at roughly  $r \lesssim 3$  Mpc for  $\sigma_8 = 0.7$  and at roughly  $r \lesssim 4$  Mpc for  $\sigma_8 = 1.0$ . Even for  $\sigma_8 = 0.5$ , the slope steepens for roughly  $r \lesssim 1.5$  Mpc. (We also computed  $\xi$  at  $\sigma_8 = 0.4$  and the results are nearly identical to  $\sigma_8 = 0.5$  except that the steepening of the slope occurs at  $r \lesssim 1.25$  Mpc rather than  $r \sim 1.5$  Mpc.) The enhancement occurs because peak par-

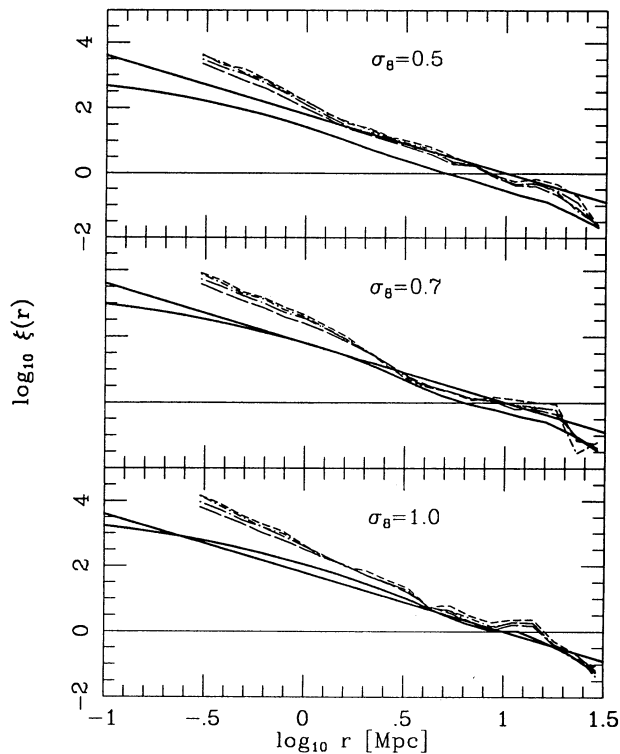


FIG. 6.— $\log_{10} \xi(r)$  for CDM 16(144<sup>3</sup>, 100, 85) where the “galaxies” are tagged from the initial density field smoothed with a Gaussian smoothing radius of  $R_s = 550$  kpc comoving ( $\nu = 2.6$ , dot-long-dashed curves;  $\nu = 3.0$ , short-dashed curves) and 880 kpc comoving ( $\nu = 2.0$ , long-dashed curves;  $\nu = 2.5$ , dot-short-dashed curves). The curved solid curve is for the mass and the solid line is the observed  $\xi$ .

ticles are more likely to be found in massive halos where the chance of a peak being above the threshold  $\nu$  is higher.

To see how peaks are associated with massive halos, we show in Figure 7 the bound particles from a massive halo ( $2.1 \times 10^{14} M_\odot$ ) at  $\sigma_8 = 0.5$  from CDM 16 (upper left panel). We use a  $512^3$  DENMAX grid which apparently has not completely resolved all substructure. We noted this problem in Paper I where we concluded that increased force resolution reveals substructure and increased DENMAX grids are required to bring out this substructure. However, in many cases there is no obvious substructure in the images of the massive halos. In the upper right panel we show peak particles that end up as bound members of the massive halo shown in the upper left panel. We see that there are many peak particles in this massive halo. (We discuss the other panels later.)

The large number of peak particles per massive halo is typical. Conservation of numbers then implies that peak particles must undersample less massive halos outside clusters. To see this quantitatively, we consider the resolved halos found by DENMAX with  $V_{\text{circ}} \geq 250 \text{ km s}^{-1}$  defined at  $R = 200$  kpc comoving at  $\sigma_8 = 0.5$ . There are 737 halos. Of these, we count the number of halos that do not contain any peak particles as bound members. For  $R_s = 550$  kpc comoving, using  $\nu = 3.0$  which yields 639 peaks, 425 resolved halos have no peak particles as bound members. (Using  $\nu = 2.9$  yields 826 peaks, and then 362 resolved halos have no peak particles as bound members.) For  $R_s = 880$  kpc comoving, using  $\nu = 2.5$  which yields 740 peaks, 355 resolved halos have no peak particles as bound members. We conclude that about half of the massive halos in the evolved, nonlinear density field contain no peak particles. This is a major failing of the peak particles as galaxy

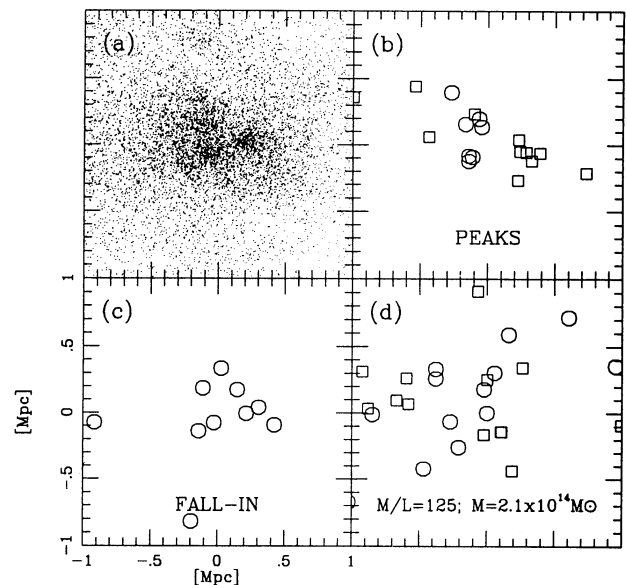


FIG. 7.—A massive halo at  $\sigma_8 = 0.5$  from CDM 16. (a) The massive halo (with mass  $2.1 \times 10^{14} M_\odot$  and  $V_{\text{circ}}[200 \text{ kpc}] = 666 \text{ km s}^{-1}$ ) found by DENMAX; note that DENMAX fails to reveal some visually distinct substructure. (b) Peak particles that are bound members of the massive halo. Circles are for  $V_{\text{circ}} \geq 250 \text{ km s}^{-1}$  and squares are for  $200 \text{ km s}^{-1} \leq V_{\text{circ}} < 250 \text{ km s}^{-1}$ . (c) Halos that formed at  $\sigma_8 = 0.2$  that fell into the massive halo. Circles are for  $V_{\text{circ}} \geq 250 \text{ km s}^{-1}$ . (d) Halos added to the massive halo assuming a mass-to-light ratio of 125; positions are randomly sampled from the massive halo; circles are for  $V_{\text{circ}} \geq 250 \text{ km s}^{-1}$  and squares are for  $192 \text{ km s}^{-1} \leq V_{\text{circ}} < 250 \text{ km s}^{-1}$ .

tracers (cf. Katz et al. 1993) and it calls into question  $N$ -body simulations that rely on peak particles in lieu of dense halos.

### 3.2. Discussion

Should we conclude from Figure 6 that the correlation function slope in the CDM model is too steep on small scales? Park (1991) presented similar studies of  $\xi(r)$  using peak particles, but he did not show the steepening of  $\xi$  within 1 Mpc. His force resolution was of order  $\sim 1$  Mpc (for a  $256^3$  grid PM simulation in a 153.6 Mpc box). However, his models show, in agreement with our results, the steepening of the slope at larger scales for  $\sigma_8 = 1.0$ . We will have to compute  $\xi(r)$  using actual resolved halos, with and without the breakup of merged massive halos, to decide whether the steepening of  $\xi(r)$  is real or an artifact of peak particles.

In any case, we conclude that the method of peak particles can give misleading results. In § 2 we found that we could only get a significant enhancement in  $\xi$  at  $\sigma_8 = 0.4$  if we broke up massive halos, but this produced far too many halos. We found that we can get the required enhancement in  $\xi$  at  $\sigma_8 = 0.5$  (the results were similar at  $\sigma_8 = 0.4$ ) using the correct number of peak particles. However, half of the actual, massive, nonlinear halos did not contain any peak particles. Because there is nothing unusual about those halos that do not contain peak particles (compared with halos of the same circular velocity that do), we cannot argue that peak particles are to be preferred over direct identification of dense resolved halos. Peak particles oversample the clusters and undersample the field. These effects enhance the two-point correlation function with fewer halos. For these reasons, we must study the CDM model using resolved dense halos, rather than peak particles, to trace galaxies.

## 4. TWO-POINT CORRELATIONS OF HALOS

### 4.1. Introduction

The preceding section has motivated a study of the two-point correlation function using resolved halos, which we undertake in this section. We use the high-resolution simulation CDM 16( $144^3$ , 100, 85) in an attempt to constrain  $\sigma_8$  based on the slope and amplitude of  $\xi(r)$ . We will find that the results depend on how merged halos are treated, so we will devote some discussion to this issue.

We show  $\xi$  computed from resolved halos at  $\sigma_8 = 0.5$ , 0.7, and 1.0 from CDM 16 in Figure 8. We use a  $512^3$  DENMAX grid, with bound particles only (see Paper I), for the remainder of this paper. We see that the correlation length,  $r_0$ , falls short of the observed value at low values of  $\sigma_8$ . Also, there is increased merging at later epochs (see Paper I); this explains why the halos are antibiased, i.e., are less clustered than the mass, on small scales. The antibiasing is stronger at later epochs and for smaller halos. This is because merging increases with increasing  $\sigma_8$  and the smallest halos merge into larger systems. Unfortunately for us, observers do not directly measure the clustering of the mass; they measure the clustering of the galaxies. However, we see that unless galaxies are clustered more strongly than the halos, we will not be able to match the observed two-point correlation function.

Carlberg & Couchman (1989) performed a simulation with  $1.2 \times 10^{11} M_\odot$  particles in a 80 Mpc box. (CDM 16 has particles with  $2.3 \times 10^{10} M_\odot$  in a 100 Mpc box.) At  $\sigma_8 = 0.54$ , using FOF to identify dark halos, they found, as we do, that the dark halos are antibiased with respect to the mass on small

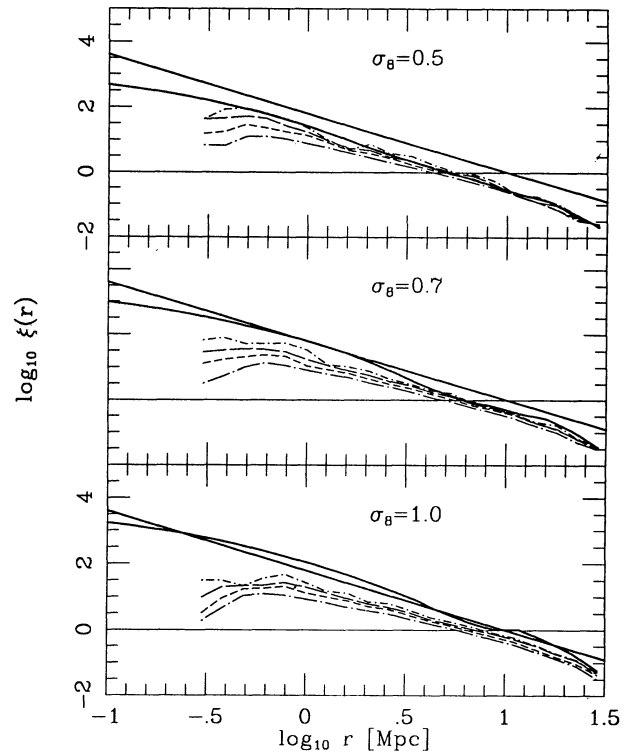


FIG. 8.— $\text{Log}_{10} \xi(r)$  for DENMAX halos from CDM 16. The solid line is the observed  $\xi$ . The curved line is for the mass. Here there is no special treatment of massive halos. The results are shown for  $V_{\text{circ}} \geq 100 \text{ km s}^{-1}$  (dot-long-dashed curves),  $V_{\text{circ}} \geq 150 \text{ km s}^{-1}$  (short-dashed curves),  $V_{\text{circ}} \geq 192 \text{ km s}^{-1}$  (long-dashed curves), and  $V_{\text{circ}} \geq 250 \text{ km s}^{-1}$  (dot-short-dashed curves).

scales and that they trace the mass on larger scales (see their Fig. 8b). Couchman & Carlberg (1992) studied more evolved models and they also found the same level of antibiasing of the dark halos with respect to the mass on small scales.

If we take these results for  $\xi$  at face value, then the  $\Omega = 1$  CDM model has serious shortcomings: the correlation length is too small for  $\sigma_8 \lesssim 0.7$ , and the correlation amplitude is too small and turns over on small scales, particularly for  $\sigma_8 \gtrsim 0.7$ . Rather than abandon the model, however, we explore the possibility that restoring merged halos might sufficiently increase  $\xi$ . This step is reasonable, because the most massive halos clearly ought to contain several galaxies. However, we will find that we create as many problems in the process as we solve!

We break up the massive halos using two techniques. The first method (fall-in method) involves finding the maximally bound particle in each halo at an earlier epoch. We identify the maximally bound particles that have fallen into massive halos representing clusters at the present epoch. The second method (mass-to-light method) involves assuming a mass-to-light ratio for the massive halos representing clusters, and then, using the observed Schechter luminosity function, assigning the appropriate number of members to the clusters. The fall-in method directly shows that smaller halos merge into larger halos, as we showed in Paper I. Perhaps dissipative effects (Katz et al. 1992; Katz & White 1993; Evrard et al. 1994) or harder forces (Dubinski & Carlberg 1991) might help these systems survive the merging process. However, because clusters exist but are overmerged in our simulations, it is reasonable to unmerge the most massive halos.



#### 4.2. Breakup of Halos: Fall-in Method

In the fall-in method we find all of the bound 512<sup>3</sup> DENMAX objects at an early epoch, which we call the *tagging era*, and we find the maximally bound particle from each of these halos. We then grab the present-day positions and velocities of these particles and we add each one to our list of present-day objects only if it is a bound member of a massive halo with present-day circular velocity (defined within a radius 200 kpc)  $\geq 350 \text{ km s}^{-1}$ . Thus, we break up the bound mass of large halos into several different objects that were distinct entities at the tagging era. Each such object is assigned the circular velocity it had at the tagging era. We also retain the massive merged halo, unless the sum of masses of the added halos exceeds its mass.

There are two arbitrary parameters in the method: the circular velocity beyond which we break up the massive halos and the epoch which we choose as the tagging era. For the former we choose  $V_{\text{circ}} = 350 \text{ km s}^{-1}$ . For larger values we found excessive numbers of halos in Paper I. We are admittedly forcing improved agreement with the observations. For the tagging era we try  $\sigma_8 = 0.2$  and  $\sigma_8 = 0.3$ . There is no ideal, single epoch since galaxy formation is a continual process. WDEF eliminated this ambiguity by finding every halo that ever formed and then by putting merging in by hand. We do not attempt to reproduce their procedure.

We show an example of the fall-in method at  $\sigma_8 = 0.5$  in the lower left panel of Figure 7. This example uses  $\sigma_8 = 0.2$  for the tagging era. Ten objects with  $V_{\text{circ}} \geq 250 \text{ km s}^{-1}$  fall into the massive halo shown in the upper left panel. When we use  $\sigma_8 = 0.3$  for the tagging era there are four halos with  $V_{\text{circ}} \geq 250 \text{ km s}^{-1}$  that fall into this massive halo. Larger values of  $\sigma_8$  contain larger objects, but many of these objects have already undergone merging.

We now examine the effect of the fall-in method on  $\xi$  at  $\sigma_8 = 0.5$ . We can see in Figure 7 that we introduce more pairs on small scales (*lower left panel*) and that we give extra weight to the massive halo (*upper left panel*). We show  $\xi$  after applying the fall-in method to CDM 16 in the top panel of Figure 9. (The  $M/\mathcal{L}$  method is discussed in the next section.) Compare these results with the results without breakup in the top panel

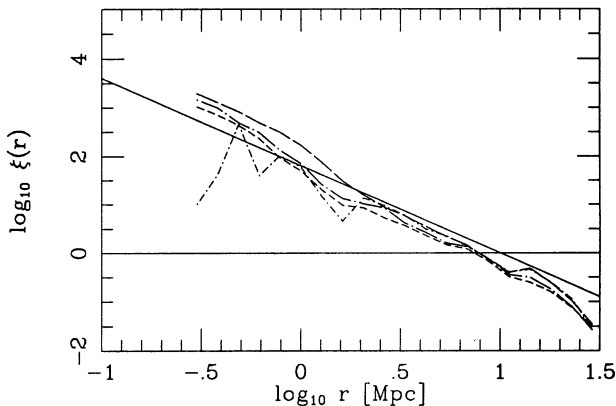


FIG. 9.— $\log_{10} \xi(r)$  for DENMAX halos from CDM 16 at  $\sigma_8 = 0.5$ . We broke up massive halos with  $V_{\text{circ}} \geq 350 \text{ km s}^{-1}$  using halos that fell in from  $\sigma_8 = 0.2$  (*dot-long-dashed curve*) and  $\sigma_8 = 0.3$  (*short-dashed curve*). We also show results assuming a mass-to-light ratio of 125 where we randomly sample the positions (*long-dashed curve*) and where we put all added halos on top of each other (*dot-short-dashed curve*). The solid line is the observed  $\xi$ .

of Figure 8. We see better agreement of the slope with the observed slope except on scales less than 1 Mpc. We also see that we increase the correlation length closer to the observed value.

The numbers of halos with no special treatment of the massive halos at  $\sigma_8 = 0.5$  are 1340 for  $V_{\text{circ}} \geq 200 \text{ km s}^{-1}$  and 737 for  $V_{\text{circ}} \geq 250 \text{ km s}^{-1}$ . The numbers from the fall-in method at  $\sigma_8 = 0.5$  are 1934 (1706) for  $V_{\text{circ}} \geq 200 \text{ km s}^{-1}$  and 1022 (940) for  $V_{\text{circ}} \geq 250 \text{ km s}^{-1}$  if we use  $\sigma_8 = 0.2$  ( $\sigma_8 = 0.3$ ) as the tagging era. There is a  $\sim 30\%$ – $40\%$  increase in the numbers of halos using the fall-in method, showing that there has been a significant amount of merging.

The fall-in method and the peak particles method produce nearly the same shape of  $\xi$  (see Fig. 6). However, the steepening of the slope occurs at  $r \sim 0.8 \text{ Mpc}$  using the fall-in method, compared with  $r \sim 1.5 \text{ Mpc}$  using the peak particles method. Both produce the wrong shape.

Notice that the feature at  $r \sim 1.5 \text{ Mpc}$  in the bottom panel of Figure 4 is more prominent than it is in Figure 9. This is because the halos are more extended using a 512<sup>3</sup> DENMAX analysis in a 100 Mpc box compared with using a 512<sup>3</sup> DENMAX analysis in a 51.2 Mpc box, as we discussed in Paper I. The effectively coarser DENMAX allows more peripheral particles. These peripheral particles make the halos bigger and introduce more pairs beyond  $\sim 1.5 \text{ Mpc}$ .

The most important difference between the fall-in method and the peak particles method is that the former requires far more halos to get the same level of enhancement as the peak particle method. This is to be expected because, as we demonstrated in §3, the method of peak particles oversamples the clusters and misses many field galaxies. If galaxies cluster like dense dark matter halos, then it would seem that the amount of clustering bias (i.e., the ratio of  $\xi$  for galaxies to that for the mass) must be less than predicted based on peak particles.

#### 4.3. Breakup of Halos: Mass-to-Light Method

As an alternative to the fall-in method for breaking up massive halos we consider an ad hoc method designed to constrain the mass-to-light ratio  $M/\mathcal{L}$  of clusters. We associate these galaxy clusters with the massive merged halos and assign each such halo the number of galaxies expected on average given a universal luminosity function. This method sacrifices all predictive power for cluster  $M/\mathcal{L}$ 's but we do not consider this a grave loss because we doubt that any reasonable attempt can be made to estimate the luminosities of galaxies in a cluster using a purely dissipationless simulation that follows only the dark matter. With the  $M/\mathcal{L}$  method, we assume only that the most massive halos should be associated with galaxy clusters and that a specific  $M/\mathcal{L}$  applies for all such clusters. This simple-minded prescription offers, at least, a useful foil for the fall-in method. Moreover, it allows us to vary the richness of clusters by varying a single number,  $M/\mathcal{L}$ . On the other hand, Ashman, Salucci, & Persic (1993) argue that observations of disk galaxies imply a variable  $M/\mathcal{L}$  which could reduce the excess richness and numbers of galaxies in clusters implied by hierarchical models assuming constant  $M/\mathcal{L}$ .

Our procedure is straightforward. We examine all halos with  $V_{\text{circ}}$  (defined at  $R = 200 \text{ kpc}$  comoving) exceeding  $350 \text{ km s}^{-1}$ . For each such halo we divide its total bound mass by a specified  $M/\mathcal{L}$  (with  $\mathcal{L}$  measured in the blue) to get the total blue luminosity in the cluster. Ramella, Geller, & Huchra (1989, hereafter RGH) find  $M/\mathcal{L} \sim 180h$  (in units of  $M_{\odot}/\mathcal{L}_{\odot}$ ) for groups in the CfA2 survey. Some clusters are estimated to have

values exceeding  $500h$ , but there is still controversy among workers in the field. Trimble (1987) gives a review.

We obtain a distribution of galaxies using the Schechter luminosity function  $\Phi(\mathcal{L})$  with parameters  $\Phi^* = 1.56 \times 10^{-2} h^3 \text{ Mpc}^{-3}$ ,  $M_{87}^* = -19.68 - 2.5 \log_{10} h^{-2}$ , and  $\alpha = -1.07$  (Efstathiou et al. 1988). The total luminosity in a volume  $V$  is

$$\mathcal{L}_{\text{total}} = V \int_0^{\infty} \mathcal{L} \Phi(\mathcal{L}) d\mathcal{L}. \quad (4.1)$$

The total number of galaxies in a volume  $V$  with a luminosity exceeding  $\mathcal{L}$  is

$$N(>\mathcal{L}, V) = V \int_{\mathcal{L}}^{\infty} \Phi(\mathcal{L}) d\mathcal{L}. \quad (4.2)$$

Combining equations (4.1) and (4.2) and defining  $x \equiv \mathcal{L}/\mathcal{L}_*$ , we get the total number of halos exceeding a luminosity  $\mathcal{L}$  in a cluster with total light  $\mathcal{L}_{\text{total}}$ :

$$N(>\mathcal{L}, \mathcal{L}_{\text{total}}) = \frac{\mathcal{L}_{\text{total}}}{\mathcal{L}_*} \frac{\int_{\mathcal{L}/\mathcal{L}_*}^{\infty} x^\alpha e^{-x} dx}{\Gamma(2+\alpha)}. \quad (4.3)$$

Colless (1989) and Schechter (1976) inform us that the same luminosity function works for rich clusters and for field galaxies within the uncertainty of the data.

We now put the steps together. We take the bound mass of one massive halo (those with  $V_{\text{circ}} \geq 350 \text{ km s}^{-1}$ ) and we divide it by a specified universal value of  $M/\mathcal{L}$ . This gives us the total luminosity emitted by the cluster:  $\mathcal{L}_{\text{total}}$ . We then add  $N(>\mathcal{L}, \mathcal{L}_{\text{total}})$  halos with luminosity exceeding  $\mathcal{L}$  to the big halo using equation (4.3). We relate  $\mathcal{L}$  to circular velocity using the Tully-Fisher (Pierce & Tully 1988) and Faber-Jackson relations (using our fit from Faber et al. 1989; see Paper I for details). We assume 70% spirals and 30% ellipticals; for the latter, the  $V_{\text{circ}}$  is corrected to  $\sigma_1$  using equation (2.2) with  $F = 1$  (no significant difference occurs if we use  $F = 1.1$ ). The value of  $\mathcal{L}$  corresponding to  $V_{\text{circ}}$  is chosen so that the number in equation (4.3) exceeding  $\mathcal{L}$  is the same as the number exceeding  $V_{\text{circ}}$ .

When we add in halos using this mass-to-light method we need to choose positions and velocities. We do this by randomly sampling the massive halos we are breaking up. In other words, if the massive halo contains  $N_h$  particles, we generate a uniform random number  $N_r$  from 1 to  $N_h$  and we use the present-day position and velocity of particle  $N_r$ . We repeat this procedure for each added halo. The breakup of the massive halo in the upper left panel of Figure 7 is shown for the mass-to-light method with random position sampling for  $M/\mathcal{L} = 125$  in the lower right panel of Figure 7. In Figure 9 we show  $\xi$  at  $\sigma_8 = 0.5$  for  $M/\mathcal{L} = 125$  where we did this random sampling (*long-dashed curve*), and where we put all added halos on top of each other at the locations of the original massive halos (*dot-dashed curve*). The results agree at larger scales, but it is essential to use the random sampling method to see the effects from close pairs. We use random sampling for the remainder of this paper.

In Figure 9 we see that the mass-to-light method produces results similar to the fall-in method and the peak particles method. We notice, however, that the slope on small scales is steeper for the mass-to-light method than for the fall-in method but comparable to the peak particles method. This is because there are more galaxies added with  $M/\mathcal{L} = 125$  than with the fall-in method. We quantify these numbers later. By varying  $M/\mathcal{L}$  we can test whether the spatial and velocity

statistics as well as numbers of halos are acceptable for a given model. These quantities are not guaranteed to all work out satisfactorily even with the freedom we allow ourselves in how massive halos are broken up. We will see, on the contrary, that small-scale galaxy clustering and velocities, combined with galaxy abundances and group multiplicities, present serious difficulties for the CDM model.

#### 4.4. Constraining $\sigma_8$ Using $\xi(r)$

In this subsection we investigate the two-point correlation function of simulated galaxies from our 100 Mpc high-resolution CDM simulation CDM 16(144<sup>3</sup>, 100, 85). Galaxies are identified with DENMAX halos except for the massive halos, which are split into several galaxies using either the fall-in method or the mass-to-light method, with  $M/\mathcal{L}$  a parameter that we can vary. The purpose is to determine whether there exists a normalization  $\sigma_8$  such that  $\xi$  for the simulated galaxies matches the observations. We vary the break-up procedure to determine the sensitivity of our conclusions to this uncertain step.

Figure 10 shows results at three epochs  $\sigma_8 = 0.5, 0.7,$  and  $1.0$ . The shape of  $\xi$  fails to match the observed  $\xi$  in all cases and this must be considered to be a serious shortcoming of the models. At  $\sigma_8 = 0.5$  the enhancement in  $\xi$  is nearly sufficient for  $M/\mathcal{L} = 50$  but the slope is too steep on small scales. Gott & Turner (1979) showed that the logarithmic slope  $-1.8$  is valid down to at least scales of  $\sim 10 \text{ kpc}$  with no indications of any features on small scales. The  $M/\mathcal{L} = 250$  case at  $\sigma_8 = 0.5$  is not too steep on small scales, but the correlation length is

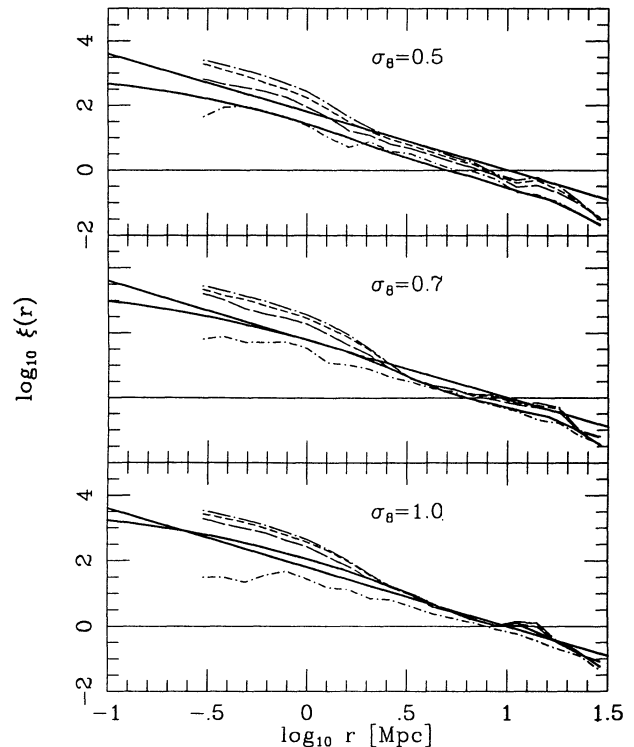


FIG. 10.— $\log_{10} \xi(r)$  for DENMAX halos with  $V_{\text{circ}} \geq 250 \text{ km s}^{-1}$  from CDM 16. We break up the massive halos ( $V_{\text{circ}} \geq 350 \text{ km s}^{-1}$ ) using mass-to-light ratios: 50 (*dot-long-dashed curves*), 125 (*short-dashed curves*), and 250 (*long-dashed curves*). The results without break-up are shown as dot-short dashed curves. The solid curves are for the mass and the solid lines are the observed  $\xi$ .

only  $\approx 7$  Mpc. For  $M/\mathcal{L} = 500$  the correlation length is  $\approx 6$  Mpc and  $\xi$  falls between the no break-up case and the  $M/\mathcal{L} = 250$  case at small scales at  $\sigma_8 = 0.5$ . The no break-up case at  $\sigma_8 = 1$  is almost acceptable, but the significant turnover on small scales does not match the observed slope and the massive halos do not look anything like observed clusters, i.e., they are single objects rather than tens of objects. At no epoch, with no treatment of halo break-up, do the simulations match the observations.

We now examine the numbers of halos and the properties of the clusters since these are central to further conclusions regarding  $\xi$ . In Table 2 we list the numbers of halos with  $V_{\text{circ}} \geq 250 \text{ km s}^{-1}$ . The numbers are for the  $(100 \text{ Mpc})^3$  volume. The numbers without break-up are in the default column; we also show numbers for  $M/\mathcal{L} = 50, 125, 250$ , and 500.

The observed number is less than 621 (563) for  $V_{\text{circ}} \geq 250 \text{ km s}^{-1}$ , assuming  $\sigma_1 = V_{\text{circ}}/(3^{1/2}/F)$  for ellipticals with  $F = 1$  ( $F = 1.1$ ). (Again, this is an overestimate because of the assumed Faber-Jackson relationship; see Paper I.) Even before breaking up the merged halos the numbers are too large; breaking up the halos leads to an even greater disagreement with observations. The numbers for  $M/\mathcal{L} = 50$  and 125 are factors  $\gtrsim 3$ –10 too high! Therefore, unless the mean  $M/\mathcal{L} \gtrsim 1000h$  for typical groups, we can safely rule out  $\sigma_8 \gtrsim 0.7$  just from the numbers shown in Table 2.

The numbers for  $M/\mathcal{L} = 250$  at  $\sigma_8 = 0.5$  are also high, but may be consistent with observations within various uncertainties. If we choose  $M/\mathcal{L} \gtrsim 250$  we partially solve the high galaxy abundance problem and the correlation function steepness problem, but we do not raise the correlation length to the observed value. Remember, WDEF found a factor of  $\sim 3$  too many halos to yield the required enhancement in  $\xi$  at  $\sigma_8 = 0.4$  (although they used a 50 Mpc box), and we see in Figure 10 that the correlation length falls short of the observed value at  $\sigma_8 = 0.5$  for  $M/\mathcal{L} = 250$ . At later epochs we can solve the steepness problem using the catalogs without breaking up the clusters, but then our simulations do not have rich clusters like the real universe.

Finally, the numbers of galaxies from the fall-in method at  $\sigma_8 = 0.5$  are comparable to the  $M/\mathcal{L} = 250$  numbers in Table 2 at  $\sigma_8 = 0.5$ . This explains why  $\xi$  at  $\sigma_8 = 0.5$  looks markedly similar for the fall-in method and for the mass-to-light method with  $M/\mathcal{L} = 250$ . This lends some support to our use of the mass-to-light method. If gaseous dissipation is able to preserve galaxies in clusters, even when the dark matter halos merge (White & Rees 1978; Katz & White 1993; Evrard et al. 1994), the CDM model might produce clusters of galaxies with  $M/\mathcal{L} \approx 250$ , in not too violent disagreement with the observations.

## 5. CLUSTERS AND THEIR RICHNESS

It is not enough for CDM or any other theory to predict the correct two-point correlation function, pairwise velocity dis-

persions, and galaxy abundances. A successful theory must also predict the correct richnesses, abundances, and mass-to-light ratios of galaxy groups and clusters. As we have noted, this test is difficult to make using a purely gravitational  $N$ -body simulation without dissipation because of the overmerging problem. However, we showed in the preceding section that a plausible scheme for undoing the overmerging is based on assigning galaxies to massive merged halos in proportion to the mass. Is it possible to do this with a reasonable value of  $M/\mathcal{L}$  so that the correct group multiplicity function (richness distribution) is obtained? Are there then too many clusters?

Let us recall first that the mean  $M/\mathcal{L}$  for  $\Omega = 1$  is  $\sim 750$  for  $h = 0.5$ . On the other hand, most dynamical measurements on cluster scales yield values smaller by a factor of 3 or more (see, e.g., Peebles 1986). While velocity bias in clusters might reduce the apparent  $M/\mathcal{L}$  to acceptable values for  $\Omega = 1$ , there exist more direct mass measurements from X-ray emission for some clusters (e.g., Hughes 1989). We will therefore examine as well how much mass is contained in our massive halos.

We compute the fraction of the total mass in our  $(100 \text{ Mpc})^3$  volume contained in massive halos at  $\sigma_8 = 0.5, 0.7$ , and 1.0 using CDM 16. We accumulate the total bound mass in all halos with  $V_{\text{circ}}$  (defined at 200 kpc comoving) exceeding  $350 \text{ km s}^{-1}$ ; these are the objects that we have been breaking up in the previous section. We find the percentage of mass contained in these objects to be 19.2% (267 objects) at  $\sigma_8 = 0.5$ ; 29.9% at  $\sigma_8 = 0.7$  (363 objects); and 39.9% (420 objects) at  $\sigma_8 = 1.0$ . These numbers are excessive when one recalls that only a few percent of galaxies are in rich clusters; see Bahcall (1979) for a review.

Since these fractions are so high, we compute a few more interesting numbers. We compute the fraction of the mass contained in objects at  $\sigma_8 = 1.0$  using larger circular velocity cutoffs. For objects with  $V_{\text{circ}} \geq 400 \text{ km s}^{-1}$  the mass fraction is 36.9% (301 objects). For objects with  $V_{\text{circ}} \geq 500 \text{ km s}^{-1}$  the mass fraction is 31.5% (170 objects). Therefore, the amount of mass contained in very massive objects is enormously high. In Paper I we learned that the cumulative mass fraction converged with increasing mass resolution if we imposed a distance cut. Therefore, we compute the mass fraction of objects above a given velocity cutoff defined at 500 kpc comoving, and we accumulate only the bound mass within 500 kpc comoving. At  $\sigma_8 = 1$  for  $V_{\text{circ}} \geq 350 \text{ km s}^{-1}$  the mass fraction is 20.2% (344 objects). At  $\sigma_8 = 1$  for  $V_{\text{circ}} \geq 500 \text{ km s}^{-1}$  the mass fraction is 15.0% (156 objects). The numbers of objects are slightly less for cutoff radii of 500 kpc comoving versus 200 kpc comoving because many of the circular velocity profiles with  $V_{\text{circ}} \sim 500 \text{ km s}^{-1}$  are actually falling slightly at these scales. However, for larger circular velocities the profiles are still rising beyond 200 kpc comoving.

There is some uncertainty in defining the bound mass of our massive halos. However, even using a conservative estimate we find that at least 15% of the mass is contained in very massive

TABLE 2  
NUMBERS OF HALOS IN A 100 MPC BOX (CDM 16) WITH  $V_{\text{circ}} \geq 250 \text{ km s}^{-1}$

$\sigma_8$	Default (no breakup)	$M/\mathcal{L} = 50$	$M/\mathcal{L} = 125$	$M/\mathcal{L} = 250$	$M/\mathcal{L} = 500$
0.5.....	737	3209	1485	948	783
0.7.....	856	4790	2101	1287	977
1.0.....	860	6197	2627	1551	1101



halos (with  $V_{\text{circ}} \geq 500 \text{ km s}^{-1}$ ) at  $\sigma_8 = 1$ . On the other hand, the percentage is not 100% so we can consider mass-to-light ratios less than 750 for our massive objects (remember that  $\Omega = 1$  demands  $M/\mathcal{L} = 750$  on average) if  $M/\mathcal{L} > 750$  for less massive objects. Unfortunately for  $\Omega = 1$  CDM, this goes against observations (Trimble 1987). One cannot argue that the missing mass is far outside galaxies in the CDM model (at least with  $\sigma_8 \gtrsim 0.5$ ) because more than half the mass is within 500 kpc from the center of a halo (cf. Paper I).

Next, we consider the richness of our handmade clusters and we impose further constraints on the mass-to-light ratios; the reader is reminded that the numbers of halos in our volume also impose constraints (see Table 2).

RGH studied groups of galaxies from the  $B(0) \leq 15.5$  CfA2 redshift survey. Redshift space projection effects may bias some group properties relative to groups selected using distance information as we do in our simulations (Nolthenius & White 1987). Nevertheless, we feel it is useful to present a preliminary analysis of the group multiplicity function in the CDM model. For our discussion in this section we convert all relevant quantities to Zwicky magnitudes using  $B(0) \approx B_T + 0.29$  (Efsthathiou et al. 1988). We replicate our  $(100 \text{ Mpc})^3$  volume using periodic boundary conditions into a  $(250 \text{ Mpc})^3$  volume. We then select a wedge corresponding to the CfA2 sky coverage: right ascension range  $8^{\text{h}} \leq \alpha \leq 17^{\text{h}}$  and declination range  $26^{\circ}5' \leq \delta < 38^{\circ}5'$ . We refer to this as the  $12^\circ$  slice. We assume  $H_0 = 50 \text{ km s}^{-1} \text{ Mpc}^{-1}$  and we impose a distance cut of  $R \leq 240 \text{ Mpc}$  in our analysis. We use actual galaxy positions rather than redshifts and we impose an apparent magnitude limit of  $B(0) \leq 15.5$ . We assume a Tully-Fisher relationship, see Paper I, converted to  $M_{B(0)}$ , where we determine the circular velocities of the halos from CDM 16 at 200 kpc comoving.

We use DENMAX to identify all halos with  $V_{\text{circ}} \geq V_{\text{circ}}^{\text{MIN}} = 50 \text{ km s}^{-1}$ ; then we use FOF to identify groups of halos in our wedge after breaking up the massive halos ( $V_{\text{circ}} \geq 350 \text{ km s}^{-1}$ ) using the mass-to-light method. We determine a FOF linking length,  $l$  in Mpc, corresponding to a given galaxy overdensity  $\delta\rho/\rho$  given by  $l^3 = 2/(n\delta\rho/\rho)$  (see, for example, Frenk et al. 1988), where  $n$  is the number density of halos with circular velocity exceeding  $V_{\text{circ}}^{\text{MIN}}$  from our original  $(100 \text{ Mpc})^3$  volume. We use FOF to identify groups of halos after breaking up the massive halos, but prior to imposing an apparent magnitude limit. Typical values of  $l$ , for  $\delta\rho/\rho = 80$ , range from 0.8 Mpc to 1 Mpc for the various assumed values of  $M/\mathcal{L}$  and  $\sigma_8$ .

We identify only groups with three or more members to be consistent with RGH. RGH chose a linking distance using a galaxy number density estimated from the observed Schechter luminosity function. However, they varied their linking length with redshift to account for the sparse sampling of galaxies at large redshift. We avoid this difficulty by applying FOF with a fixed linking length prior to applying an apparent magnitude limit. We then apply the apparent magnitude limit to the resulting group catalog in a manner described below.

For field halos, i.e., those that are not in groups with three or more members, we simply compute  $M_{B(0)}$  using the Tully-Fisher relationship, and we remove those with  $B(0) > 15.5$ . For the halos in groups we apply the following procedure. If the group member is not created from the breakup of a massive halo, then we eliminate it if  $B(0) > 15.5$ . For group members that are created from the breakup of a massive halo, we remove all of them and replace them by the number of halos determined from equation (4.3) for an assumed, universal  $M/\mathcal{L}$ . The lower luminosity limit in equation (4.3) is computed from

$15.5 - M_{B(0)} = 5 \log_{10} d + 25.0$ , where  $d$  is the distance to the group centroid in Mpc. Note that here we do not need to relate luminosity to  $V_{\text{circ}}$  in equation (4.3). However, to be consistent with our use of  $V_{\text{circ}}^{\text{MIN}}$ , we never allow  $\mathcal{L}$  to fall below  $\mathcal{L}_{\text{min}}$  determined from  $V_{\text{circ}}^{\text{MIN}}$  using the Tully-Fisher relationship.

The basic parameters in the group finding algorithm are the galaxy overdensity  $\delta\rho/\rho$  used to determine the linking parameter, the faint cut  $V_{\text{circ}}^{\text{MIN}}$ , the mass-to-light ratio  $M/\mathcal{L}$  used to break up the massive halos, and the circular velocity cutoff above which we break up massive halos. We discuss these four parameters here.

1. We report results using  $\delta\rho/\rho = 80$ , the middle value considered by RGH, since we see the same levels of variation with  $\delta\rho/\rho$  as reported by RGH and our conclusions do not depend critically on its value.

2. We report results for  $V_{\text{circ}}^{\text{MIN}} = 50 \text{ km s}^{-1}$ . Our results do not depend sensitively on  $V_{\text{circ}}^{\text{MIN}}$  because the low-mass galaxies quickly fall out of sight. For example, in a case where we identify 1555 field galaxies in our  $12^\circ$  slice with an apparent magnitude limit, only 233 have  $V_{\text{circ}} \leq 125 \text{ km s}^{-1}$  and only 62 have  $V_{\text{circ}} \leq 75 \text{ km s}^{-1}$ . This is encouraging since we found in Paper I that we had factors  $\sim 2$ – $3$  too many halos compared with the observations for  $V_{\text{circ}} \leq 125 \text{ km s}^{-1}$ . In a magnitude-limited survey we would not be swamped by low-mass halos.

3. We report results using  $M/\mathcal{L} = 125, 250$ , and  $500$ . From a list of 36 groups, RGH found a median  $M/\mathcal{L}$  of  $178h = 89$  for  $h = 0.5$ . We choose large values of  $M/\mathcal{L}$  because, as we will see, even  $M/\mathcal{L} = 125$  produces groups that are too rich.

4. There is some arbitrariness to the value of  $V_{\text{circ}}$  above which we break up the massive halos. We report results using  $V_{\text{circ}} = 350 \text{ km s}^{-1}$ . If we raise this value we get too many isolated massive halos (see Paper I) which are too big to represent individual galaxies. On the other hand, the numbers of halos added quickly approaches zero below  $V_{\text{circ}} = 350 \text{ km s}^{-1}$  for the  $M/\mathcal{L}$  studied here.

The results from our simulations are shown in Table 3. We report numbers from RGH for the full  $12^\circ$  slice, but we impose a redshift cut of  $12,000 \text{ km s}^{-1}$ . RGH studied only groups with centroids  $\leq 12,000 \text{ km s}^{-1}$ . We report numbers from the simulations for the full  $12^\circ$  slice for  $R \leq 240 \text{ Mpc}$ . The table shows the number of groups  $N_{\text{groups}}$ , identified with three or more members, with 10 or more members, and with 20 or more members. We also show the number of galaxies,  $N_{\text{galaxies}}$ , in the field, i.e., those that are not in groups with three or more members. We estimate the number of CfA2 field galaxies within  $12,000 \text{ km s}^{-1}$  as follows. The CfA2 catalog has 1766 galaxies and we estimate from Figure 1 in RGH that  $\approx 100$  galaxies are beyond  $12,000 \text{ km s}^{-1}$ . RGH found 778 galaxies in groups with three or more members, and only a handful of these galaxies are beyond  $12,000 \text{ km s}^{-1}$ . Therefore, the number of field galaxies within  $12,000 \text{ km s}^{-1}$  in the CfA2 catalog is approximately  $1766 - 788 - 100 \sim 900$  galaxies. The last entry in the table,  $N_{1/2}$ , is a richness statistic defined later. The reader is cautioned that RGH estimate that  $\gtrsim 30\%$  of the groups with three or four members might be an artifact of projection effects.

We can draw several important conclusions from the results shown in Table 3. If we do not break up the massive halos, then we do not have enough groups and there are no groups with 10 or more members. Therefore, we need to break up our massive halos if our simulated universe is to contain groups comparable to the observed numbers! In all cases we have too many field galaxies. We demonstrated earlier that these are not

TABLE 3  
GROUP STATISTICS IN A 12° SLICE FROM CDM 16

Data	$\sigma_8$	$N_{\text{groups}} \geq 3$ Members	$N_{\text{groups}} \geq 10$ Members	$N_{\text{groups}} \geq 20$ Members	$N_{\text{galaxies}}$ in Field <sup>a</sup>	$N_{\text{galaxies}}$ in Groups <sup>b</sup>	$N_{1/2}$ <sup>c</sup>
CfA2 .....	N.A.	128	7	2	900	778	6
No Breakup .....	0.5	30	0	0	1910	106	<3
$M/L = 125$ .....	0.5	136	36	17	1622	1366	19
$M/L = 250$ .....	0.5	79	19	5	1579	633	11
$M/L = 500$ .....	0.5	56	6	2	1555	322	6
No Breakup .....	0.7	25	0	0	1901	83	<3
$M/L = 125$ .....	0.7	197	37	16	1589	1933	19
$M/L = 250$ .....	0.7	106	17	8	1523	843	14
$M/L = 500$ .....	0.7	58	8	3	1470	370	9
No Breakup .....	1.0	58	0	0	1660	197	<3
$M/L = 125$ .....	1.0	237	55	25	1452	2843	22
$M/L = 250$ .....	1.0	138	27	11	1341	1307	16
$M/L = 500$ .....	1.0	83	11	5	1300	610	13

<sup>a</sup> Field galaxies are galaxies not in groups with three or more members.

<sup>b</sup> Groups must have three or more members.

<sup>c</sup> The value of  $N_{\text{members}}$  where the cumulative number of galaxies in groups (eq. [4.6]) reaches  $\frac{1}{2}$  its maximum value.

dominated by faint galaxies. However, in Paper I we found that we had the correct number of halos with circular velocities between  $150 \text{ km s}^{-1}$  and  $350 \text{ km s}^{-1}$ . The reason for this discrepancy is that here we apply only the Tully-Fisher relationship to the halos (i.e., we are treating all halos as spirals) rather than a combination of the Tully-Fisher relationship and the Faber-Jackson relationship as we did in Paper I. Applying the Tully-Fisher relationship to elliptical galaxies, which tend to be the most massive halos, makes the halos appear brighter than they really are. On the other hand, most of our group members result from the breakup of massive halos where we do not need to assume a relationship between circular velocity and luminosity. Because of this problem, we should give more emphasis to the richness of our groups than to the apparent excess of field galaxies. (We use the Tully-Fisher relation only for field galaxies; massive halos are broken into galaxies based on an assumed mass-to-light ratio.)

We can constrain  $M/L \gtrsim 125 = 250h$  based on the number of groups with three or more members and the total number of galaxies in all groups with three or more members. For  $\sigma_8 = 1$ ,  $M/L$  must be  $\sim 250 = 500h$ . In most cases, however, we still have too many rich groups with 50 or more members. We should note that because the observed number of groups with three or four members may be contaminated by projection effects, the total numbers of objects in groups could be smaller by  $\gtrsim 30\%$  (see RGH). This would lower the observed numbers in groups and, by definition, raises the observed numbers in the field, although it does not solve the problem of too many rich groups.

To further quantify the richness of our groups, we compare the cumulative number of galaxies in groups with the estimates from RGH for the CfA2 survey. The cumulative number of galaxies in groups is defined by RGH as

$$N_{\text{galaxies}}(\leq N_{\text{members}}) \equiv \sum_{N=3}^{N=N_{\text{members}}} N N_g(N), \quad (5.1)$$

where  $N_{\text{galaxies}}(\leq N_{\text{members}})$  is the total number of galaxies contained in all groups with three to  $N_{\text{members}}$  members and  $N_g(N)$  is the number of groups containing  $N$  members. The results are shown in Figure 11 using  $M/L = 125, 250$ , and  $500$ , and the no breakup cases, at  $\sigma_8 = 0.5, 0.7$ , and  $1.0$ . Figure 11 is computed for a  $6^\circ$  slice (we divide the numbers from our  $12^\circ$  slice by two) to compare with RGH using a  $6^\circ$  (their Fig. 2).

We clearly see the dramatic shortcoming of the no breakup cases at all epochs. When the massive halos are broken up we find groups that are richer than observed by RGH; the rise in the predicted cumulative galaxy number is also generally slower than the results for the CfA2 survey indicating that our

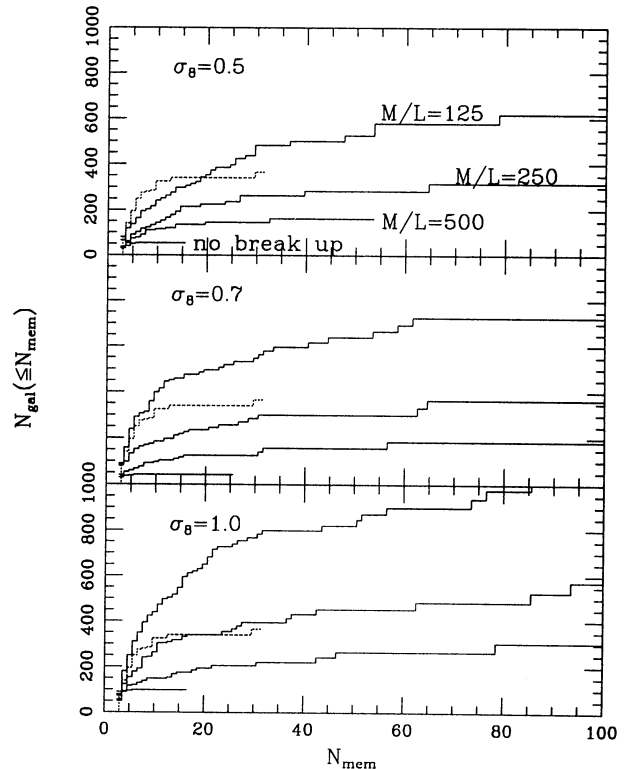


FIG. 11.—Cumulative number of galaxies in groups with three or more members; see eq. (5.1). We break up the massive halos using the mass-to-light method with  $M/L = 125$  (top lines), 250, and 500; the higher curves are for the smaller values of  $M/L$ . The lowest curves are results without breaking up the massive halos. We assume  $\delta\rho/\rho = 80$  to determine the FOF linking length. The results are for a  $6^\circ$  wedge out to  $R = 240$  Mpc with a magnitude limit  $B(0) = 15.5$ . (Note well, we divide the numbers from a  $12^\circ$  wedge in the simulation by two. This explains why the jumps in the solid histograms are half the value implied by  $N_{\text{mem}}$ .) The RGH results for a  $6^\circ$  wedge are shown for comparison as dashed histograms.

group members are concentrated in relatively larger groups. A useful statistic is  $N_{1/2}$  shown in Table 3. This is the value of  $N_{\text{members}}$  where the cumulative number of galaxies in groups reaches  $\frac{1}{2}$  its maximum value. The value of  $N_{1/2}$  indicates that we need  $M/\mathcal{L} \gtrsim 250$ . We can rule out  $M/\mathcal{L} = 125$ . The remaining question is whether or not nature can hide a lot of mass; this will be an important consideration when we study velocities in the next section.

## 6. HALO PAIR VELOCITY DISPERSIONS AND CLUSTERS

We now consider constraints on  $\sigma_8$  from CDM 16(144<sup>3</sup>, 100, 85) based on pairwise velocity dispersions of the resolved halos. We address the following questions: What is  $\sigma_p$  for the halos without the breakup of massive halos? How do we assign velocities to halos added to the massive halos, and what is the effect on  $\sigma_p$ ? Is there a linear normalization of the  $\Omega = 1$  CDM model,  $\sigma_8$ , when the pairwise velocity dispersions agree with the observations?

### 6.1. Constraining $\sigma_8$ Using $\sigma_p(r)$ of Simulated Halos

The pairwise velocity dispersions of the halos from CDM 16 without breaking up the massive halos are shown in Figure 12 at  $\sigma_8 = 0.5, 0.7$ , and 1.0. We define the circular velocities at 200 kpc comoving, and we show results for  $V_{\text{circ}} \geq 100, 150, 192$ , and 250  $\text{km s}^{-1}$ .

The open symbols are the observed estimates from the Davis & Peebles (1983, hereafter DP) analysis of the CfA  $B(0) \leq 14.5$  redshift survey. The different symbols are for different model-

ing parameters. The best estimates are open circles with 1  $\sigma$  error bars (shown as vertical lines). The squares are for a different set of modeling parameters, and the triangles are results with three clusters removed. The details are not important for our purposes; the scatter is small compared with the  $\sigma_8$  dependence of  $\sigma_p$ . The results at  $r \sim 10$  Mpc are the least accurate because of distortions from peculiar motions. CDM 16 has a Plummer softening of 65 kpc comoving which affects small scales. For these reasons, we will focus our comparisons at  $r \sim 1, 2.2$ , and 4.6 Mpc.

DP removed all galaxies with  $M_{B(0)} > -18.5 + 5 \log_{10} h = -20$ . If we convert this to the  $B_T$  system and use the Tully-Fisher relationship (see Paper I), this corresponds to removing all halos with  $V_{\text{circ}} \lesssim 175 \text{ km s}^{-1}$ . We study all halos with  $V_{\text{circ}} \geq 150 \text{ km s}^{-1}$  and  $V_{\text{circ}} \geq 250 \text{ km s}^{-1}$ . The former is important since the pairwise velocity dispersions increase with increasing circular velocity cutoff and simulated dispersions are higher than the observed estimates at  $\sigma_8 \gtrsim 0.7$ . If we are to rule out any values of  $\sigma_8$ , it is better to be conservative.

Based on Figure 12, observational data constrains  $\sigma_8 \lesssim 0.7$ . The case  $\sigma_8 = 0.5$  is an excellent match to the observed data. The results are in reasonable agreement with the observed data at  $\sigma_8 = 0.7$  for  $V_{\text{circ}} \geq 100$  and marginally for  $V_{\text{circ}} \geq 150 \text{ km s}^{-1}$ . The case  $\sigma_8 = 1.0$  is ruled out; the pairwise velocity dispersions are too high by factors  $\sim 1.5$  for  $r \gtrsim 1$  Mpc. Note that this is true even though there is a velocity bias of about a factor of 2!

There are two important issues we need to consider. We notice that the pairwise velocity dispersions are significantly lower for the resolved halos than for the mass. This velocity bias was discussed in § 2.4. We also need to compare our results with Couchman & Carlberg (1992, hereafter CC) who investigated  $\sigma_8 \approx 1.0$  and a 2 million particle  $P^3M$  simulation in a 200 Mpc box. CC used a different definition to normalize the linear CDM power spectrum; their  $b_1 = 0.8$  corresponds to  $\sigma_8 \approx 1.0$ . CC assumed  $\Omega = 1$ ,  $H_0 = 50 \text{ km s}^{-1} \text{ Mpc}^{-1}$ , and their particle mass is  $2.65 \times 10^{11} M_\odot$  compared with our particle mass of  $2.3 \times 10^{10} M_\odot$  for CDM 16.

CC found a pairwise velocity dispersion for halos with  $M \gtrsim 2.1 \times 10^{12} M_\odot$  at 1 Mpc of  $\sim 490 \text{ km s}^{-1}$  in agreement with our results for the lower circular velocity cutoffs. CC found a pairwise velocity dispersion for the mass of  $\sim 2300 \text{ km s}^{-1} / 3^{1/2} \approx 1325 \text{ km s}^{-1}$  at 1 Mpc; this is again in agreement with our results. CC did not report pairwise velocity dispersions on larger scales where we find the disparity with the observations to be large. CC also found that their halos have smaller two-point correlations than the mass; this is in agreement with our result presented § 4.

We argued in § 4 that we need to break up massive halos into clusters to remove the turnover of  $\zeta$  on small scales and to enhance the correlation length, and in § 5 because clusters really exist in our universe. We also argued in § 2.4 that using the center of momentum of resolved halos significantly reduced the pairwise velocity dispersions compared with the mass since a significant number of high-velocity particles are contained in a few massive halos. For these reasons it is important to consider the effect on  $\sigma_p$  of breaking up the massive halos before further conclusions can be drawn.

We use the mass-to-light method to break up the halos with  $V_{\text{circ}} \geq 350 \text{ km s}^{-1}$ , randomly sampling the positions and the velocities of the massive halos to assign positions and velocities to the added halos. The results are shown in Figure 13. We see immediately that the pairwise velocity dispersion for the halos

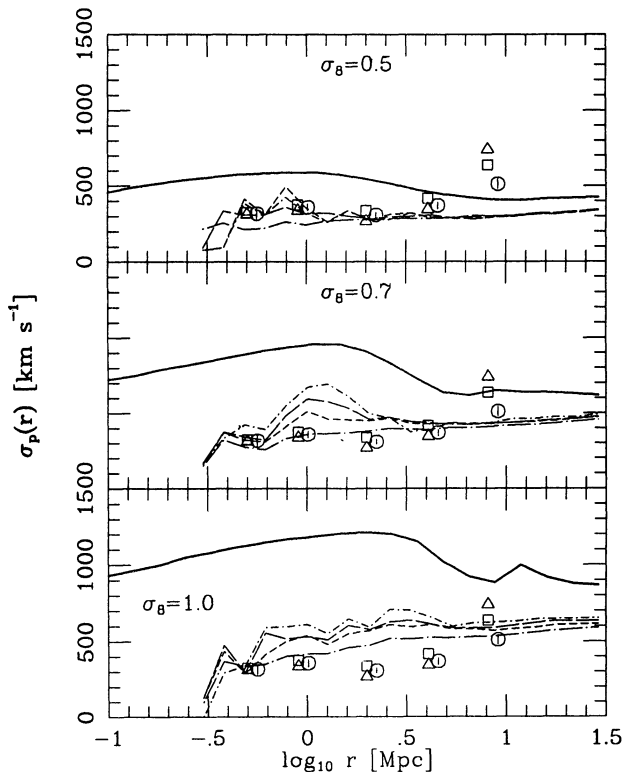


FIG. 12.— $\sigma_p$  for DENMAX halos from CDM 16. Here there is no special treatment of massive halos. We show circular velocity cutoffs of 100  $\text{km s}^{-1}$  (dot-long-dashed curves), 150  $\text{km s}^{-1}$  (short-dashed curves), 192  $\text{km s}^{-1}$  (long-dashed curves), and 250  $\text{km s}^{-1}$  (dot-short-dashed curves). The observed estimates are shown as open symbols for various modeling parameters from Davis & Peebles (1983). The solid curves are for the mass.



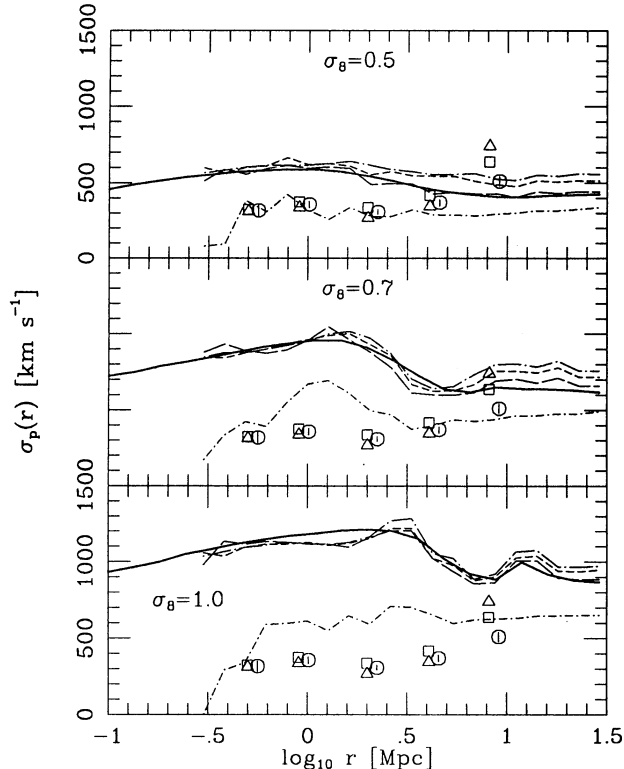


FIG. 13.— $\sigma_p$  for DENMAX halos with  $V_{\text{circ}} \geq 250 \text{ km s}^{-1}$  from CDM 16. We break up the massive halos ( $V_{\text{circ}} \geq 350 \text{ km s}^{-1}$ ) using the mass-to-light method:  $M/L = 50$  (dot-long-dashed curves),  $M/L = 125$  (short-dashed curves),  $M/L = 250$  (long-dashed curves). (The positions and velocities of the added halos are assigned using random sampling.) The dot-short-dashed curves are without breakup. The solid curves are for the mass.

now traces that for the mass. We have introduced a significant number of pairs with high-velocity dispersions; the added cluster members sample massive halos which have high-velocity dispersions. These results indicate that the pairwise velocity dispersions are too high at  $\sigma_8 = 0.5, 0.7,$  and  $1.0$  if we break up the massive halos.

CC did not report the high pairwise velocity dispersions associated with clusters. They found that merging decreases the numbers of halos in high-dispersion regions, and they referenced Bertschinger & Gelb (1991) where we first discussed why this effect can significantly reduce pairwise velocity dispersions. However, CC did include a prescription for preserving merged systems as distinct halos found by FOF, but they commented that only  $\sim 20\%$  of their “galaxy precursors” survive as distinct “galaxies.” A group analysis of the CC data, as we have done in § 5, is needed to estimate their group multiplicity function. Because our default catalogs (no breakup) reveal  $\sigma_p$  in agreement with CC at 1 Mpc, we suspect that they would see higher  $\sigma_p$  if they had the requisite group multiplicity function.

Before we can rule out any values of  $\sigma_8$  we must examine lower circular velocity cutoffs. We must also consider the possibility that the velocity dispersions of galaxies in clusters can be less than the velocity dispersions of the dark matter. Finally, we must consider  $M/L = 500$  at  $\sigma_8 = 0.5$  which compares favorably with the observed properties of groups of galaxies. These tests are the focus of the next subsection.

## 6.2. Velocities of Added Cluster Members

In the previous section we randomly sampled the velocities of the particles in the massive halos to assign velocities to the added cluster members. An alternative method is to use the one-dimensional velocity dispersion of each massive halo as the rms for random numbers.

We compute  $\sigma_1$  at 200 kpc comoving;  $\sigma_1$  is very flat at these scales (see Paper I). We label this quantity as  $\sigma_1^{(\text{MH})}$ ; MH is used to denote the original massive halo. We label the  $i$ th (for  $i = x, y, z$ ) component of the center-of-momentum velocity of the massive halo as  $v_i^{(\text{MH})}$ . We then compute three Gaussian random numbers,  $r_i$ , with mean zero and a one-dimensional standard deviation  $\sigma_1^{(\text{MH})}$  for each cluster member. We define the velocity of the added cluster member as

$$v_i(\text{cluster member}) = v_i^{(\text{MH})} + \beta^{1/2} r_i, \quad (6.1)$$

for some constant  $\beta \leq 1$  discussed next.

The quantity  $\beta$  is the ratio of “galaxy temperature” to the virial or gas temperature (see Sarazin 1988; Evrard 1990). The “galaxy temperature” is a measure of the kinetic energy of the galaxies and the gas temperature is directly related, in hydrostatic equilibrium, to the gravitational potential well. Observational estimates yield  $\beta \sim 0.8$  (Evrard 1990) with a range 0.4 to 1 (Table 2 of Sarazin 1988).

We show  $\sigma_p$  in Figures 14a and 14b using this method to assign velocities to the added cluster members with  $\beta = 1, 0.8,$  and  $0.25$ . We use the mass-to-light method to break up the halos with  $V_{\text{circ}} \geq 350 \text{ km s}^{-1}$ . We use  $M/L = 250$  in Figure 14a,  $M/L = 500$  in Figure 14b, and in both cases we consider halos with  $V_{\text{circ}} \geq 150 \text{ km s}^{-1}$ ; these values, and  $\beta = 0.25$ , are chosen specifically to give low estimates of  $\sigma_p$ . We want to know how much we need to “push” the parameters to match the DP estimates of the pairwise velocity dispersions. Admittedly,  $\beta = 0.25$  is far below the lowest observational estimates ( $\sim 0.4$  at best), and is only shown as a final, futile attempt to save CDM! The solid curves are for the mass. The  $\beta = 1$  cases are comparable to the  $M/L = 250$  cases using the random sampling method of Figure 13. Here they are slightly lower because we show halos with  $V_{\text{circ}} \geq 150 \text{ km s}^{-1}$  rather than for  $V_{\text{circ}} \geq 250 \text{ km s}^{-1}$  used in Figure 13. We conclude that even small  $\beta$  cannot save  $\sigma_8 \geq 0.7$ . The case  $\sigma_8 = 0.5$  still has pairwise velocity dispersions that are high compared with the observations for  $M/L = 250$  and the model requires  $\beta \lesssim 0.25$  which is extremely small compared with observed estimates. The same conclusion holds for  $M/L = 500$  at  $\sigma_8 = 0.5$  except that the  $\beta = 0.25$  case is a reasonable match to the observed pairwise velocity dispersions. However, as mentioned earlier,  $\beta = 0.25$  is far below any observed estimate from real clusters.

DP computed pairwise velocity dispersions,  $\sigma_p(r)$ , with and without the removal of three clusters: Virgo, Coma, and A1367. The triangles in Figures 14a, b, c are the DP numbers computed without these three clusters, yet their effect is small except for the 10 Mpc bin where the numbers are unreliable. However, the effect is not small for  $\sigma_8 = 1$  CDM as we now show. The CDM model is plagued with far too many massive halos (see Paper I) and too many rich clusters (see § 5 of this paper). In CDM 16, we find 17 halos with  $V_{\text{circ}} > 1000 \text{ km s}^{-1}$  at  $\sigma_8 = 1$  (involving 395 galaxies with  $V_{\text{circ}} \geq 150 \text{ km s}^{-1}$  using the mass-to-light method with  $M/L = 500$ ). We find two halos with  $V_{\text{circ}} > 1000 \text{ km s}^{-1}$  at  $\sigma_8 = 0.7$  (involving 57 galaxies with  $V_{\text{circ}} \geq 150 \text{ km s}^{-1}$ , again using the mass-to-light method with  $M/L = 500$ ). Last, we find no halos with  $V_{\text{circ}} > 1000 \text{ km s}^{-1}$  at  $\sigma_8 = 0.5$ .

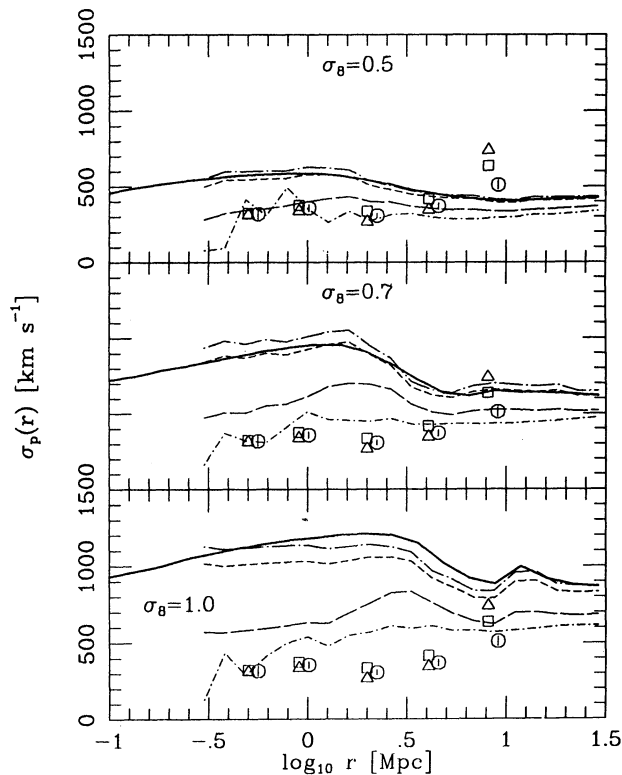


FIG. 14a

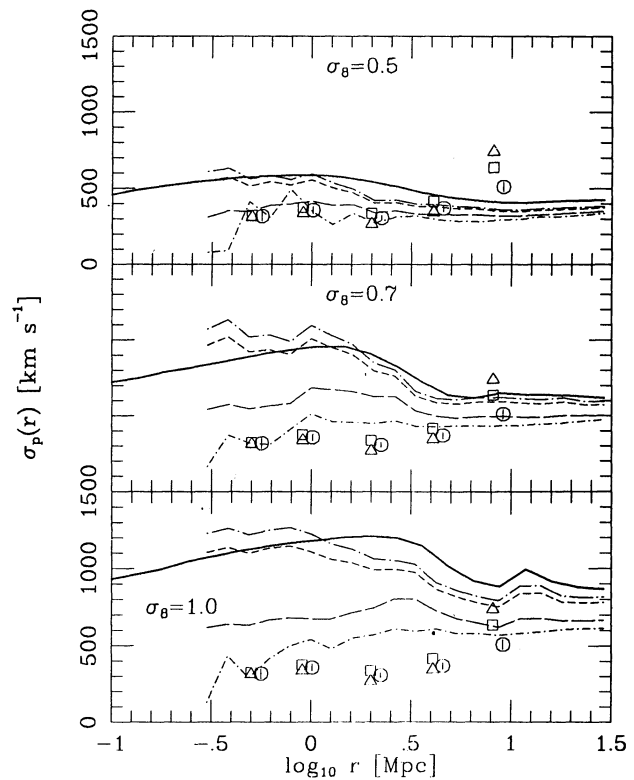


FIG. 14b

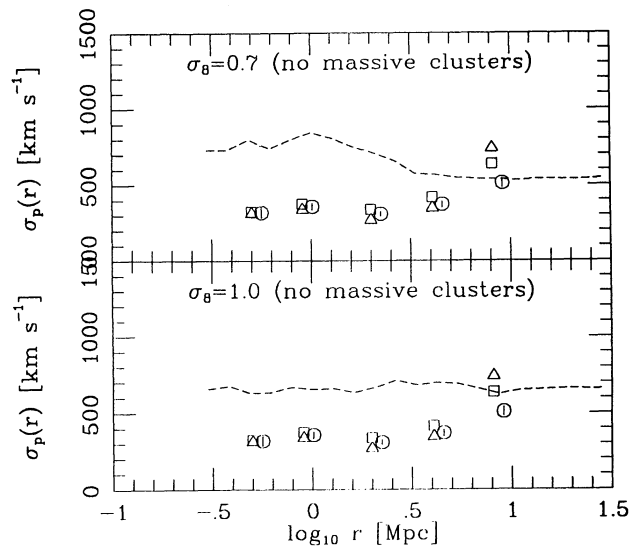


FIG. 14c

FIG. 14.— $\sigma_p$  for DENMAX halos with  $V_{\text{circ}} \geq 150 \text{ km s}^{-1}$  from CDM 16. The massive halos ( $V_{\text{circ}} \geq 350 \text{ km s}^{-1}$ ) are broken up with (a)  $M/\mathcal{L} = 250$  and (b)  $M/\mathcal{L} = 500$ . The solid curves are for the mass. The results without breakup are the dot-short-dashed curves. The velocities of added members are generated from the central velocity dispersions and  $\beta$  (eq. [6.1]). The  $M/\mathcal{L}$  curves are for  $\beta = 1.0$  (dot-long-dashed curves),  $\beta = 0.8$  (short-dashed curves), and  $\beta = 0.25$  (long-dashed curves). (c)  $\sigma_p(r)$  for CDM 16 halos with  $V_{\text{circ}} \geq 150 \text{ km s}^{-1}$ , removing those halos (and their progeny) with  $V_{\text{circ}} \geq 1000 \text{ km s}^{-1}$ . Halos with  $350 \text{ km s}^{-1} \leq V_{\text{circ}} \leq 1000 \text{ km s}^{-1}$  are broken up with  $\beta = 0.8$  and  $M/\mathcal{L} = 500$ .

We now compute  $\sigma_p(r)$  without the inclusion of halos (or added members) with  $V_{\text{circ}} > 1000 \text{ km s}^{-1}$ . The results are shown in Figure 14c for halos with  $V_{\text{circ}} \geq 150 \text{ km s}^{-1}$ ,  $\beta = 0.8$ , and  $M/\mathcal{L} = 500$  applied to halos with  $V_{\text{circ}} \geq 350 \text{ km s}^{-1}$  (cf. Fig. 14b which includes all clusters). The effect is substantial at  $\sigma_8 = 1$ ; nevertheless,  $\sigma_p(r)$  is still too large by a factor  $\sim 2$  compared with observations for  $r \gtrsim 1 \text{ Mpc}$ . In order to significantly reduce  $\sigma_p(r)$  at  $\sigma_8 = 1$  we must (1) assume a ridiculously small  $\beta$  and (2) remove an extreme number of rich clusters. Even so, these effects are not strong enough to reconcile a  $\sigma_8 \geq 0.7$  CDM universe with observed small-scale pairwise velocity dispersions of galaxies.

As a final comment, we note some recent work that is relevant to the formation of galaxies in massive clusters in the CDM model. Katz & White (1993) (see also Evrard et al. 1994) have performed a gas dynamical CDM simulation with  $\Omega = 1$ ,  $H_0 = 50 \text{ km s}^{-1} \text{ Mpc}^{-1}$ , and  $\sigma_8 = 0.4$ . They simulated a volume of space containing a massive halo found from a previous dark matter only simulation. The object at  $z = 0$  ( $z = 1/a - 1$ ;  $a = 1$  at  $\sigma_8 = 0.4$ ) had a mass of  $1.83 \times 10^{14} M_\odot$  and a circular velocity of  $945 \text{ km s}^{-1}$ ; it formed from the merging of two massive subclumps. The gas dynamical simulation, assuming a 10-to-1 ratio of dark matter mass-to-gas mass, was evolved to  $z = 0.13$ . During the course of the simulation eight galaxies formed, but by  $z = 0.13$  only four galaxies had survived the merging process. (Each of these four galaxies had a cold gas mass exceeding  $1.9 \times 10^{11} M_\odot$ .) Estimates of  $\beta$ , with these limited statistics, were  $\beta \sim 1$  at  $z = 0.6$  and  $\beta \sim 0.4$  at  $z = 0.13$ .

This work is interesting because it demonstrates that some galaxies can survive the merging process. However, this fact does not solve the problems demonstrated in this paper. Our mass-to-light method predicts that a  $1.83 \times 10^{14} M_\odot$  object

should contain four halos with  $V_{\text{circ}} \geq 250 \text{ km s}^{-1}$  if  $M/\mathcal{L} \sim 500 = 1000h$ . This is a factor of 5 too few compared with more typical  $M/\mathcal{L} \lesssim 200h$ ; see Trimble (1987).

Although the gas dynamical simulation of Katz & White (1993) demonstrated that some galaxies can survive the merging process in a single massive halo, it did not demonstrate that the  $\Omega = 1$  CDM model can successfully make clusters of galaxies with reasonable mass-to-light ratios. Furthermore, it did not demonstrate that CDM with gas dynamics can solve the problems we have found in this paper. We leave open the possibility that a full scale CDM simulation with gas dynamics might significantly alter the distribution of luminous galaxies compared with dark matter halos. However, it is difficult to imagine how this could avoid the problems associated with having too many massive halos where galaxies are sure to form as seen in the cosmological gas simulations of Katz et al. (1992).

On the other hand, we have found that  $M/\mathcal{L} = 500$  at  $\sigma_8 = 0.5$  might solve some of the problems with the models. The numbers of halos and group properties were in good agreement with the observations. However, the correlation length ( $r_0 \sim 6 \text{ Mpc}$ ) fell short of the observed value  $r_0 = 10 \text{ Mpc}$ . We found in this section that the velocities for  $M/\mathcal{L} \gtrsim 250$  at  $\sigma_8 = 0.5$  are marginally consistent with the observed pairwise velocity dispersions and are in good agreement with the observed pairwise velocity dispersions for  $\beta \lesssim 0.25$  and  $M/\mathcal{L} = 500$ . If CDM is to survive on small scales, nature must conspire to hide a lot of dark matter.

## 7. CONCLUSIONS

There appears to be no linear normalization of the power spectrum for the  $\Omega = 1$  CDM model that can simultaneously match the observed numbers, the spatial clustering, and the pairwise velocity dispersion of resolve dark matter halos. The problems are especially serious for the large amplitude ( $\sigma_8 \sim 1.0$ ) implied by the recent *COBE* DMR anisotropy results.

We must break up the massive halos if our catalogs are to contain groups of galaxies like the observed universe. If we study the models without breaking up the massive halos, then we find that the two-point correlation function turns over on small scales and the correlation length is too small except for  $\sigma_8 \sim 1$  where the turnover on small scales is particularly severe. We also find that the pairwise velocity dispersions constrain  $\sigma_8 \leq 0.5$  despite the fact that there is a velocity bias of a factor  $\sim 2$ .

We paid considerable attention to massive halos which might represent groups of galaxies. Breaking up these massive halos into groups of galaxies removes the turnover of the two-point correlation function on small scales and it increases the correlation length on larger scales. Unfortunately, the groups do more harm than good unless we assume very high mass-to-light ratios. They significantly increase the number of halos, they give the wrong shape of the two-point correlation func-

tion, they significantly increase the pairwise velocity dispersions, and they make groups that are too rich for reasonable mass-to-light ratios. Our estimates constrain the models to very high mass-to-light ratios  $\sim 1000h$ , although the precise values are uncertain. Factors such as (1)  $\beta$ , (2) how much of the bound mass should be used to estimate the group luminosity (i.e., the mass out to a given distance from the group center), and (3) variable mass-to-light ratios, all complicate the interpretation of our estimated  $M/\mathcal{L}$ . The combined uncertainty can be as much as a factor of  $\sim 2$ . However, there is increasing evidence from X-ray studies of clusters that dark matter is not hidden in the outskirts of galaxy clusters (e.g., Sciama, Salucci, & Persic 1992 and references therein).

The problems associated with  $\sigma_8 \gtrsim 0.4$  are clear. In agreement with White et al. (1987), we found that we needed to restore halos in massive systems to get the required two-point correlation length for  $\sigma_8 = 0.4$ . However, the fact that the model then had a factor  $\sim 3$  too many halos and produced the wrong shape of the two-point correlation function is a serious shortcoming of the model. We also studied models with  $\sigma_8 > 0.5$ . In agreement with Couchman & Carlberg (1992) we found a velocity bias of a factor  $\sim 2$  for  $\sigma_8 = 1$ . However, restoring the merged halos in massive systems which have high-velocity dispersions significantly increased the pairwise velocity dispersions. We can rule out  $\sigma_8 \gtrsim 0.7$ ; even  $\sigma_8 = 0.5$  required a ratio of galaxy to virial temperature  $\beta \lesssim 0.25$  which is too small compared with observed estimates. Removal of the most massive halos (with  $V_{\text{circ}} \geq 1000 \text{ km s}^{-1}$ ) can reduce pairwise velocity dispersions, but the effect is too little to save CDM with  $\sigma_8 = 1$ .

If we live in an  $\Omega = 1$  universe, nature (or clever humans) must learn to hide large amounts of dark matter. Gas dynamical simulations probably will not solve the problems we have found unless our assumptions regarding sites of galaxy formation and galaxy luminosities from the dark matter are significantly wrong.

This research was conducted using the Cornell National Supercomputer Facility, a resource of the Center for Theory and Simulation in Science and Engineering at Cornell University, which receives major funding from the National Science Foundation and IBM Corporation, with additional support from New York State and members of its Corporate Research Institute. We appreciate the programming assistance of CNSF consultant Paul Schwarz. We thank Neal Katz for useful discussions on clusters, and David Weinberg and Paul Schechter for stimulating discussions. This work was supported by NSF grant AST 90-01762 and in part by the DOE and the NASA at Fermilab through grant NAGW-2381.

The DENMAX halo catalogs and full particle data sets are available for the simulations used in this paper. Interested workers may send e-mail to [bertschinger@mit.edu](mailto:bertschinger@mit.edu).

## REFERENCES

- Adams, F. C., Bond, J. R., Freese, K., Frieman, J. A., & Olinto, A. V. 1993, *Phys. Rev. D*, 47, 426  
 Ashman, K. M., Salucci, P., & Persic, M. 1993, *MNRAS*, 260, 610  
 Bahcall, N. A. 1979, *ARA&A*, 15, 505  
 Bardeen, J. M., Bond, J. R., Kaiser, N., & Szalay, A. S. 1986, *ApJ*, 300, 15  
 Bertschinger, E. 1992, in *New Insights into the Universe*, ed. V. J. Martinez, M. Portilla, & D. Saez (New York: Springer-Verlag), 65  
 Bertschinger, E., & Gelb, J. M. 1991, *Computers in Physics*, 5, 164  
 Bertschinger, E., & Juszkiewicz, R. 1988, *ApJ*, 334, L59  
 Carlberg, R. G. 1991, *ApJ*, 367, 385  
 Carlberg, R. G., & Couchman, H. M. P. 1989, *ApJ*, 340, 47  
 Carlberg, R. G., Couchman, H. M. P., & Thomas, P. 1990, *ApJ*, 352, L29  
 Cen, R. Y., & Ostriker, J. P. 1992a, *ApJ*, 393, 22  
 ———. 1992b, *ApJ*, 399, L113  
 Colless, M. 1989, *MNRAS*, 237, 799  
 Couchman, H. M. P., & Carlberg, R. 1992, *ApJ*, 389, 453 (CC)  
 Davis, M., Efstathiou, G., Frenk, C. S., & White, S. D. M. 1985, *ApJ*, 292, 371 (DEFW)  
 Davis, M., & Peebles, P. J. E. 1983, *ApJ*, 267, 465 (DP)  
 Dubinski, J., & Carlberg, R. G. 1991, *ApJ*, 378, 496



- Efstathiou, G., Bond, J. R., & White, S. D. M. 1992, MNRAS, 258, 1P  
 Efstathiou, G., Ellis, R. S., & Peterson, B. A. 1988, MNRAS, 232, 431  
 Evrard, A. E. 1990, ApJ, 363, 349  
 Evrard, A. E., Summers, F. J., & Davis, M. 1994, ApJ, 422, 11  
 Faber, S. M., & Burstein, D. 1988, in Large-Scale Motions in the Universe, ed. V. C. Rubin & G. V. Coyne (Princeton: Princeton Univ. Press), 115  
 Faber, S. M., Wegner, G., Burstein, D., Davies, R. L., Dressler, A., Lynden-Bell, D., & Terlevich, R. J. 1989, ApJS, 69, 763  
 Frenk, C. S., White, S. D. M., Davis, M., & Efstathiou, G. 1988, ApJ, 327, 507  
 Gelb, J. M. 1992, MIT Ph.D. thesis  
 Gelb, J. M., & Bertschinger, E. 1994, ApJ, 436, 467 (Paper I)  
 Gelb, J. M., Gradwohl, B., & Frieman, J. 1993, ApJ, 403, L5  
 Gott, J. R., & Turner, E. L. 1979, ApJ, 232, L79  
 Holtzman, J. A. 1989, ApJS, 71, 1  
 Hughes, J. P. 1989, ApJ, 337, 21  
 Kaiser, N. 1984, ApJ, 284, L9  
 Katz, N., Hernquist, L., & Weinberg, D. H. 1992, ApJ, 399, L109  
 Katz, N., Quinn, T., & Gelb, J. M. 1993, MNRAS, 265, 689  
 Katz, N., & White, S. D. M., 1993, ApJ, 412, 455  
 Maddox, S. J., Efstathiou, G., Sutherland, W. J., & Loveday, J. 1990, MNRAS, 242, 43  
 Nolthenius, R., & White, S. D. M. 1987, MNRAS, 225, 505  
 Park, C. 1990, MNRAS, 242, 59  
 ———. 1991, MNRAS, 251, 167  
 Peebles, P. J. E. 1982, ApJ, 263, L1  
 ———. 1986, Nature, 321, 27  
 Pierce, M. J., & Tully, B. 1988, ApJ, 330, 579  
 Ramella, M., Geller, M. J., & Huchra, J. P. 1989, ApJ, 344, 57 (RGH)  
 Sarazin, C. L. 1988, X-Ray Emission from Clusters of Galaxies (Cambridge: Cambridge Univ. Press)  
 Saunders, W., et al. 1991, Nature, 349, 32  
 Schechter, P. L. 1976, ApJ, 203, 297  
 Sciamia, D. W., Salucci, P., & Persic, M. 1992, Nature, 358, 718  
 Smoot, G. F., et al. 1992, ApJ, 396, L1  
 Trimble, V. 1987, ARA&A, 25, 425  
 White, S. D. M., Davis, M., Efstathiou, G., & Frenk, C. S. 1987, Nature, 330, 451 (WDEF)  
 White, S. D. M., & Rees, M. J. 1978, MNRAS, 183, 341  
 Wright, E. L., et al. 1992, ApJ, 396, L13  
 Vogeley, M. S., Park, C., Geller, M. J., & Huchra, J. P. 1992, ApJ, 391, L5